First in Class Dual Non-ATP-Competitive Glycogen Synthase Kinase 3β/Histone Deacetylase Inhibitors as a Potential Therapeutic to Treat Alzheimer's Disease

First in Class Dual Non-ATP Competitive Glycogen Synthase Kinase 3β/Histone Deacetylase Inhibitors as a Potential Therapeutic to Treat Alzheimer's Disease

Journal:	*ACS Chemical Neuroscience*
Manuscript ID	cn-2024-000615.R2
Manuscript Type:	Letter
Date Submitted by the Author:	n/a
Complete List of Authors:	Santini, Alan; University of Bologna Tassinari, Elisa; University of Bologna Poeta, Eleonora; Universita degli Studi di Bologna, Pharmacy and Biotechnology Loi, Manuela; University of Bologna Ciani, Elisabetta; Univ Bologna Trazzi, Stefania; University of Bologna Piccarducci, Rebecca; Università di Pisa, Department of Pharmacy Daniele, Simona; Università di Pisa, Department of Pharmacy Martini, Claudia; Universita degli Studi di Pisa, Department of Pharmacy Pagliarani, Barbara; Università di Bologna Tarozzi, Andrea; University of Bologna, Dept. for Life Quality Studies Bersani, Matteo; University of Turin, Department of Drug Science and Technology Spyrakis, Francesca; University of Turin, Department of Drug Science and Technolgy Dankova, Daniela; University of Copenhagen, Drug design and pharmacology Olsen, Christian; Kobenhavns Universitet Sundhedsvidenskabelige Fakultet, Center for Biopharmaceuticals Soldati, Roberto; University, Chemistry Tumiatti, Vincenzo; Universita degli Studi di Bologna, Department of Pharmaceutical Sciences Montanari, Serena; Universita degli Studi di Bologna, De Simone, Angela; Universita degli Studi di Torino, Dipartimento di Scienza e Tecnologia del Farmaco Milelli, Andrea; Alma Mater Studiorum, University of Bologna, Department for Life Quality Studies

First in Class Dual Non-ATP Competitive Glycogen Synthase Kinase 3β/Histone Deacetylase Inhibitors as a Potential Therapeutic to Treat Alzheimer's Disease

Alan Santini,[1] Elisa Tassinari,[1] Eleonora Poeta,[2] Manuela Loi,[3] Elisabetta Ciani,[3] Stefania Trazzi,[3] Rebecca Piccarducci,[4] Simona Daniele,[4] Claudia Martini,[4] Barbara Pagliarani,[1] Andrea Tarozzi,[1] Matteo Bersani,[5] Francesca Spyrakis,[5] Daniela Danková,[6] Christian A. Olsen,[6] Roberto Soldati,[1] Vincenzo Tumiatti,[1] Serena Montanari,[1] Angela De Simone,[5*] and Andrea Milelli[1*]

1 Department for Life Quality Studies, Alma Mater Studiorum-University of Bologna, Corso d'Augusto 237, 47921 Rimini, Italy

2 Department of Pharmacy and Biotechnology, Alma Mater Studiorum-University of Bologna, Via Belmeloro 6, 40126 Bologna, Italy

3 Department of Biomedical and Neuromotor Science, Alma Mater Studiorum-University of Bologna, Piazza di Porta S. Donato, 2, 40126 Bologna, Italy

4 Department of Pharmacy, University of Pisa, Via Bonanno Pisano, 6, 56126 Pisa, Italy

5 Department of Drug Science and Technology, University of Turin, Via Pietro Giuria 9, 10125 Turin, Italy

6 Center for Biopharmaceuticals & Department of Drug Design and Pharmacology, Faculty of Health and Medical Sciences, University of Copenhagen, Jagtvej 160, DK-2100, Copenhagen, Denmark

Corresponding Authors:
Angela De Simone, angela.desimone@unito.it
Andrea Milelli, andrea.milelli3@unibo.it

Keywords. Alzheimer's disease; Neuroprotection; Multitarget Drugs; Glycogen Synthase Kinase 3β, Histone Deacetylase.

Abstract

Despite recent FDA approvals, Alzheimer's Disease (AD) still represents an unmet medical need. Among the different available therapeutic approaches, the development of multi-target molecules represents one of the most widely pursued. In this work, we present a second generation of dual ligands directed towards highly networked targets that are deeply involved in the development of the disease, namely Histone Deacetylases (HDACs) and Glycogen Synthase Kinase 3β (GSK-3β). The synthesized compounds are highly potent GSK-3β, HDAC2, and HDAC6 inhibitors with IC_{50}s in the nanomolar range. Among them, compound **4** inhibits histone H3 and tubulin acetylation at 0.1 micromolar concentration, blocks hyperphosphorylation of tau protein, and shows interesting immunomodulatory and neuroprotective properties. These features, together with its ability to cross the blood brain barrier and its favorable physical-chemical properties, make compound **4** a promising hit for the development of innovative disease-modifying agents.

Introduction

Around 60-80% of total dementia cases worldwide are caused by Alzheimer's Disease (AD) that is a multifactorial progressive disease for which a resolutive cure is currently not available. Due to the different intrinsic issues related to the pathology, AD has been considered the "black hole" of the drug discovery industry for a long time.[1] Since it is considered as the result of the systemic breakdown of different physiological networks, the goal of a successful therapy could be to restore the perturbed networks through the use of chemical entities, *i.e.*, Multitarget Drugs (MTDs), able to modulate multiple key targets involved in the onset of the disease.[2] There is a clear consensus that the chance of developing successful MTDs increases if they are directed towards "networked" targets.[3] Following this principle, in 2019 we reported the first-in-class MTD able to modulate Glycogen Synthase Kinase 3β (GSK-3β) and Histone Deacetylases (HDACs),[4] which are deeply involved in the pathogenesis of AD.[5 6, 7 8 9 10 11] In particular, GSK-3β is the main kinase involved in the hyperphosphorylation of tau protein,[12] leading to the formation of neurofibrillary tangles, one of the two hallmarks of AD.[6] Moreover, over-activity of GSK-3β accounts for memory impairment, increased β-amyloid production and local plaque-associated microglial-mediated inflammatory responses.[8 9 13] On the other hand, HDACs modulate both gene expression and the functions of several non-histone proteins, such as tau. Due to the involvement of HDACs in neuronal survival, and cognitive processes,[10] HDAC inhibitors (HDACIs) have been suggested as innovative (neuroprotective) agents for the treatment of neurodegenerative disorders such as AD.[11] Although HDAC2 and 6 are the isoforms more closely related to AD,[14 15] also other isoforms have been implicated, albeit with various degrees of involvement, in neurodegeneration.[16] The only exception is HDAC1 that seems to have a protective role.[17] For these reasons, in addition to the use of pan-HDAC inhibitors, such as vorinostat, nowadays many drug discovery programs aim to obtain isoform-selective HDACIs. However, although possible, it is very difficult to achieve such selectivity due to the high degree of structural similarity between HDAC isoforms. Interestingly, GSK-3β and HDACs are strictly networked and several connections have been reported among them.[18 19 20] This

provided us with the basis for the design and synthesis of a series of dual GSK-3β/HDAC inhibitors, characterized by an ATP-competitive binding mode relative to GSK-3β.[4] These compounds proved to be highly effective *in vitro* and *in cell*[4] and also in an *in vivo* model of cyclin-dependent kinase-like 5 (CDKL5) deficiency disorder.[4, 21]

Based on the above considerations, and with the aim of developing a second generation of dual inhibitors, herein we report the design, synthesis, and preliminary biological evaluations of the first set of dual *non-ATP competitive* GSK-3β/HDAC inhibitors.

Results and Discussions

Design. To design dual GSK-3β/HDAC inhibitors, we sought to combine in a single chemical entity the pharmacophoric groups responsible for binding to GSK-3β, in a non-ATP competitive manner, and to HDACs. In this work, we focused on non-ATP competitive behavior since such inhibitors, by binding to not conserved residues, offer greater selectivity and reduced toxicity compared to ATP-competitive inhibitors, as they are likely to have less off-target effects. It is well known that HDAC inhibition requires the presence of three different structural features: a zinc binding group (ZBG), a linker, and a CAP group, usually a large (hetero)aromatic surface that establishes additional interactions with the enzyme. Thanks to this peculiarity, it is possible to obtain MTDs by introducing, as CAP group, a structure that is responsible for a second biological activity.[5] To this end, we focused on tideglusib, the first non-ATP competitive inhibitor[22] that, in a pilot study, showed a satisfactory safety profile and a significant improvement in cognition compared to placebo-patients.[23] Structurally, tideglusib consists of a thiazolidindione nucleus bearing two different substituents: a benzyl and a naphthyl group. Recently, we have observed that a chain may be introduced at the benzyl para-position of tideglusib, by means of an amide linkage, without significant loss of the inhibitory activity.[24] Therefore, considering the structure of HDACIs,[25] we designed a small library of molecules possessing a hydroxamic acid, as ZBG, and a substituted thiazolidindione as CAP group. As reported

in Figure 1, different substituents were introduced to study the Structure-Activity Relationships (SAR) of the designed molecules and obtain a potential hit compound.

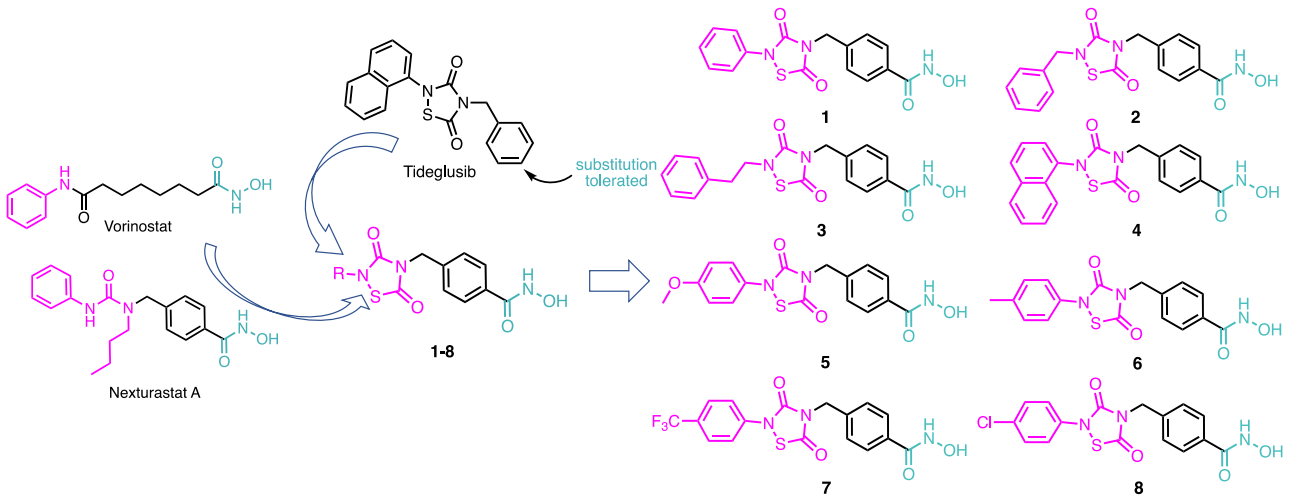

Figure 1. Drug design leading to dual non-ATP competitive GSK-3β/HDACs inhibitors. Referring to HDACs pharmacophore features, the CAP group is colored in magenta, the linker in black and the zinc-binding group in green.

Synthesis. For the synthesis of compounds **1-8** a straightforward synthetic strategy was developed as reported in Scheme 1. Briefly, **9**[24] was subjected to a sequence involving cyclization with the commercially available substituted isocyanate, in presence of sulfuryl chloride, followed by oxidation of the obtained product in atmospheric oxygen to produce compounds **10-17**. This last process represents the diversity-creation step of the synthesis. The thiadiazolidinones **10-17** were then deprotected in trifluoroacetic acid to obtain **18-25** that were subjected to amidation with tetrahydropyrane-protected hydroxylamine to install the hydroxamic acid (**26-33**). Final acidic hydrolysis led to the target compounds **1-8**.

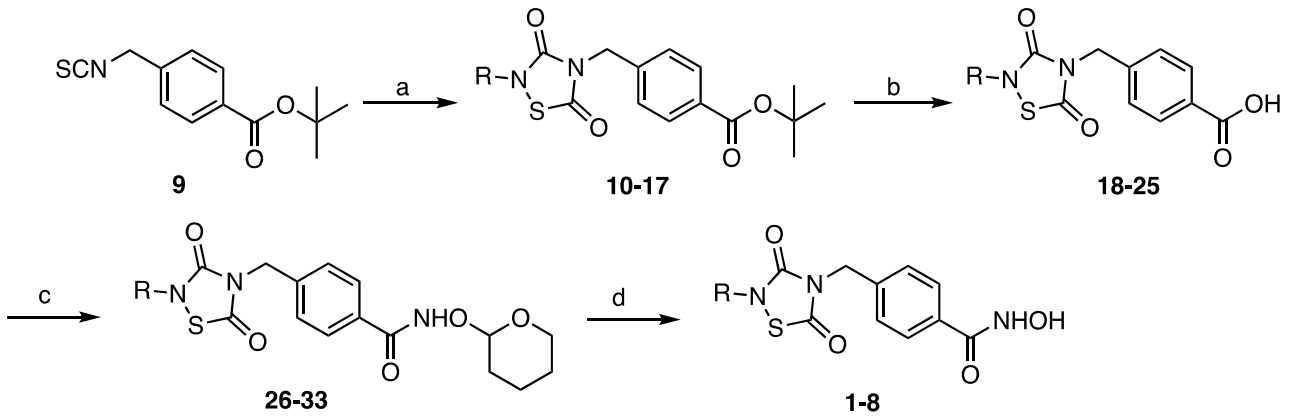

Scheme 1. a) substituted isocyanate R-NCO, sulfuryl dichloride, THF, rt, 12h, N_2 then air, THF, rt, 30 min, 29-77% yields; b) TFA, DCM, rt, 12h, 41-86% yields; c) O-(Tetrahydro-2H-pyran-2-yl)hydroxylamine, EDCI, HOBT, DMF, rt, 12h, 51-85% yields; d) TFA, DCM, rt, 12h, 34-74% yields.

In Vitro Enzymes Inhibition. Compounds **1-8** underwent parallel evaluation for their ability to inhibit GSK-3β, HDAC2, and HDAC6, in comparison to parent compounds. The compounds were first screened by enzymatic assays at 1 μM concentration; for the compounds showing an inhibitory activity higher than 50%, at this concentration, the IC_{50} was determined by evaluating the inhibitory activity at different concentrations (Table SI1 and Table 1).

Table 1. Effects of compounds **1-8**, tideglusib, vorinostat and nexturastat A, on GSK-3β, HDAC2, and HDAC6 activity.

Compounds	IC_{50} (μM)[a]		
	GSK-3β	HDAC2	HDAC6
1	n.d.[b]	n.d.[b]	n.d.[b]
2	n.d.[b]	n.d.[b]	n.d.[b]
3	0.176±0.019	0.023±0.003	0.096±0.005
4	0.142±0.006	0.030±0.005	0.045 ±0.050
5	0.084±0.020	0.002±2E-[6]	0.255±0.007

6	0.127±0.007	0.011±0.002	0.222±0.012
7	n.d.[b]	n.d.[b]	n.d.[b]
8	0.107±0.021	0.031±0.004	0.074±0.001
Tideglusib	0.200±0.015	n.d.[b]	n.d.[b]
Vorinostat	n.d.[b]	0.120±0.007	0.160±0.020
Nexturastat A	n.d.[b]	n.d.[b]	0.005±0.001[c]

[a.] IC_{50} values are defined as the drug concentration that reduces target activity by 50% and are reported as a mean value of three or more determinations; [b.] not determined, see Table SI1; [c.] data from ref. [25]

As reported in Table SI1, among the different compounds only three show an inhibitory activity lower than 50% at 1 μM concentration: compound **1** characterized by the phenyl substituent on the cyclic nitrogen, compound **2** characterized by the benzyl substituent and compound **7** characterized by the p-trifluoromethylphenyl substituent. Therefore, IC_{50}s were determined for compounds **3-6** and **8** (Table 1). Regarding GSK-3β, all the compounds showed inhibitory activity in the nanomolar range of concentrations, displaying an activity similar or superior to the reference inhibitor. In particular, the most active compound of the series was **5** (IC_{50} = 0.084 μM) characterized by the p-methoxyphenyl substituent. Good inhibitory activity was also reported for **8** (IC_{50} = 0.107 μM), **6** (IC_{50} = 0.127 μM), and **4** (IC_{50} = 0.142 μM) which carries the p-naphthyl substituent, the same of tideglusib. Based on these results, we can assume that the introduction of the hydroxamic acid in the para position of the benzyl group does not have any significant detrimental effect on the activity but, on the contrary, may increase the inhibitory potential. To the best of our knowledge, these are among the most potent thiadiazolidinones reported as GSK-3β inhibitors to date.[22, 26]

Regarding HDAC2 and 6, the designed compounds, with exception of **1**, **2**, and **7**, turned out to be very potent inhibitors with IC_{50} values in the nanomolar range of concentrations, and showed similar or superior activity compared to the reference inhibitor vorinostat. Compound **5** is a potent and

selective HDAC2 inhibitor (HDAC2 = 0.002 μM, HDAC6 = 0.255 μM; selectivity index HDAC2/HDAC6 = 127) followed by **6** (IC_{50} = 0.011 μM), **3** (IC_{50} = 0.023 μM) and **4** (IC_{50} = 0.030 μM). Regarding HDAC6, the most potent compound of the series is compound **4** (IC_{50} = 0.023 μM), followed by **8** (IC_{50} = 0.074 μM) and **3** (IC_{50} = 0.096 μM).

Based on the GSK-3β/HDACs inhibitory data and due to the more balanced inhibitory profile showed, we progressed compound **4** in the following steps of our pipeline.

Kinetic Analysis. To elucidate the inhibitory mechanism of compound **4** on GSK-3β, the Lineweaver-Burk plots of enzyme kinetics, varying ATP (from 1 to 50 μM) or GSM (from 6.25 to 25 μM) and inhibitor concentrations, were derived. The analysis of the plot reported in Figure 2 reveal compound **4** as ATP non-competitive inhibitor. Indeed, the intercept of the plot is on the x axis. On the contrary, the constant intercept of the plot on the vertical axis, obtained varying GSM and maintaining the ATP concentration constant, reveals a competitive mechanism of action of **4** for the substrate binding with a K_i value of 57.96 nM.

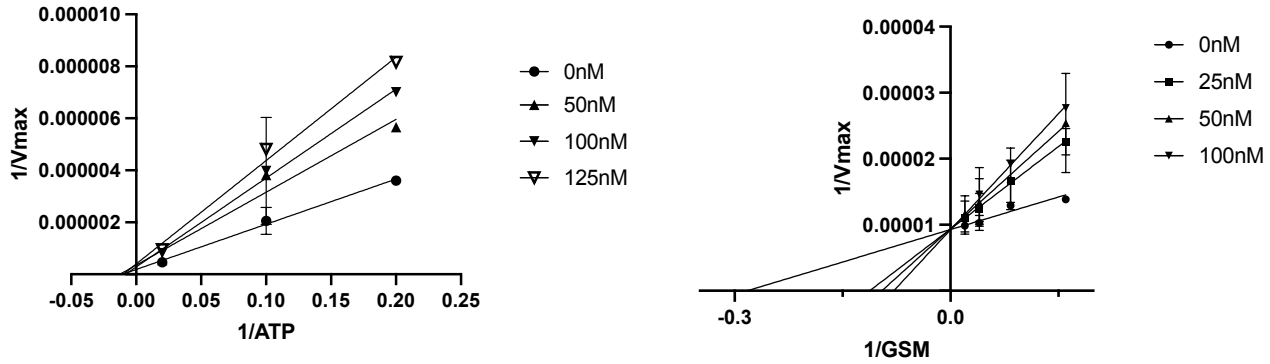

Figure 2. Kinetic data for the compound **4**. a) ATP concentration in the reaction mixture varied from 1 to 50 μM. Compounds concentrations used are depicted in the plot, and the concentration of GSM was kept constant at 25 μM. b) GSM concentration in the reaction mixture varied from 6.25 to 50 μM. Compounds concentrations used are depicted in the plot, and the concentration of ATP was kept constant at 1 μM. Each point is the mean of two different experiments, both analyzed in duplicate.

HDACs isoform selectivity. To investigate the HDAC isoforms selectivity of compound **4**, we performed end-point inhibition assays against HDAC1–9 and 11 and K_i values were determined by using the Cheng-Prusoff equation and assuming fast-on/fast-off kinetics. As shown in Table 2, compound **4** is non-selective, exhibiting potent inhibition of HDAC1–3 (Class I) and 6 (Class IIa) in the nanomolar range (K_i values: HDAC1 = 4 nM, HDAC2 = 6 nM, HDAC3 = 5.7 nM, HDAC6 = 4.2 nM). The remaining class I HDAC (HDAC8) was inhibited at 20-fold lower potency (K_i = 0.105 μM) than HDAC1–3, and K_i values were not determined for the class IIa HDACs 4, 5, 7, 9 and class IV HDAC11 as the inhibitors did not reach full inhibition at the highest measured concentration.

Table 2. K_i values for compound **4** against HDAC1–9 and 11 isoforms.

Compound **4**			
HDAC isoform	K_i (μM)[a]	HDAC isoform	K_i (μM)[a]
HDAC1	0.0040 ± 0.0007	HDAC6	0.0042 ± 0.0003
HDAC2	0.0060 ± 0.0013	HDAC7	5% at 10 μM[b]
HDAC3	0.0057 ± 0.0008	HDAC8	0.105 ± 0.007
HDAC4	35% at 10 μM[b]	HDAC9	40% at 10 μM[b]
HDAC5	50% at 10 μM[b]	HDAC11	40% at 10 μM[b]

[a] Values are reported as the mean ± standard deviation based on three individual assays performed in technical duplicate. [b] % residual activity.

Computational analysis. To gain insights into the mechanism of dual GSK-3β/HDAC inhibition and to elucidate the binding mode of compounds **1-8**, molecular docking calculations were performed on HDAC2 and HDAC6. Unfortunately, we were not able to perform any simulation for GSK-3β, considering the non-competitive nature of the inhibitors towards the kinase and the absence of structural information on the binding site. Similarly to the reported crystal structures, in all docking poses, the inhibitors are involved in H-bonds with His145, His146 and Tyr308 in HDAC2 and with

His610, His611 and Tyr782 in HDAC6 (Figure 3 and SI1). The central common scaffold and the terminal substituted aromatic ring interact through hydrophobic contacts with the several residues lining the pocket (Figure 3 and SI1), as His33, Pro34, Phe155, Phe210, Leu276 and Tyr308 in HDAC2 and His500, Pro501, Phe620, Phe680, Leu749 and Tyr782 in HDAC6. No other polar contacts were identified for the series of inhibitors, except for compound **5**, also able to H-bond to Arg275 and Asn494 in HDAC2 and HDAC6, respectively (Figure 3). According to the structures deposited in PDB,[27] several capping moieties of HDAC2 and HDAC6 inhibitors interact with residues in the L1-L2 loop region. The size and electronic properties of this region differ among HDAC isoforms, likely, providing criteria for designing HDAC selective inhibitors. According to the protein surface electrostatic potential and MIF analysis of the inhibitor binding pocket (Figure SI2), the L1-L2 region resulted wider and more hydrophobic in HDAC6 with respect to the narrower and polar sub-pocket observed in HDAC2. Indeed, in inhibition assays, small derivatives **5** and **6** showed selectivity towards HDAC2, whereas larger compounds **3, 4** and **8** resulted to be less selective (see Table 1). Docking simulations were able to reproduce this trend in most of the cases, showing, for example, unstable poses in HDAC2 for bulky compound **4,** with the naphthyl ring being more exposed towards the solvent (Figure SI1A) with respect to the pose obtained in HDAC6 (Figure SI1B). However, in the case of compound **5**, docking analyses were not sufficient to provide an explanation for the two order of magnitude higher activity reported for HDAC2. Therefore, with the aim of explaining compound **5** HDAC2 selectivity, we performed a 200ns MD simulation of **5** in complex with both isoforms, using as starting point the obtained docking poses. The MD trajectories highlighted a higher stability of compound **5** in the polar HDAC2 L1-L2 loop region, as shown in the contact map (Figure SI3) and reported in the analysis of the inhibitor solvent accessible surface area (SASA) plot (Figure SI4). RMSD (Figure SI5) and H-bond occupancy analyses (Figure SI6) were also carried out, confirming the stability of the protein structures in the simulation time-scale and the conservation of key interactions for hydroxamate binding in HDACs, respectively.

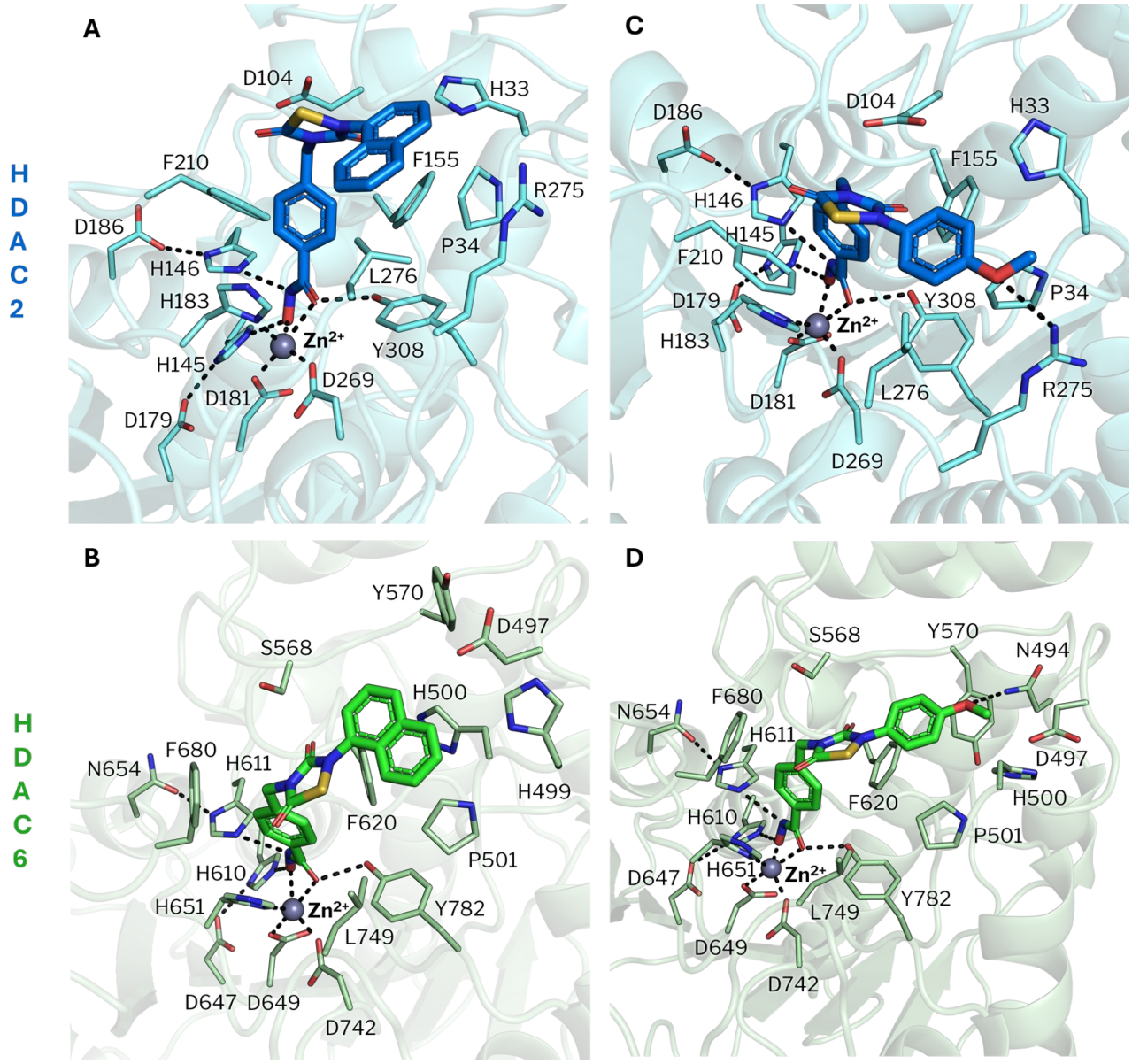

Figure 3. Docking poses of compounds **4** and **5** in HDAC2 and HDAC6.

Cytotoxicity and in-cell enzymes inhibition. Considering that (neuro)toxicity of AD drug candidates has been a drawback for clinical translation, the cytotoxicity of compound **4** was evaluated in neuronal SH-SY5Y cells in comparison to reference compounds (Figure SI7). Viability was measured using the MTT (3-(4,5-dimethylthiazol-2-yl)-2,5-diphenyl-tetraziolium bromide) reduction assay after 24 h of treatment with various concentrations of compound **4** and reference compounds. Significant cytotoxicity was showed at a concentration higher than 25 µM only. (Figure SI7).

To evaluate whether the *in vitro* inhibitory activities translate into intracellular inhibition, cell-based assays were carried out. The effects of compound **4**, tideglusib and nexturastat A, on GSK-3β serine-9 (Ser9) phosphorylation (the inactive form of the kinase) and on the acetylation levels of α-tubulin and histone H3 (biochemical markers for HDAC6 and HDAC2 activity, respectively), were determined using western blotting analysis (Figures 4a and SI8). SH-SY5Y cells were treated for 24 h with different concentrations of the compounds. Compound **4** was able to induce a dose-dependent increase in phospho-GSK-3β (Ser9) levels, comparable to that induced by tideglusib (see Figure SI8).[28] Consistently with previous evidence on other selective HDAC6 inhibitors,[29] treatment with nexturastat A also induced a slight increase of the inactivated form of GSK-3β (Figure SI8). Compound **4** was able to induce a dose-dependent increase in the acetylation levels of both histone H3 and tubulin, albeit to a different extent. Indeed, while the effect on histone H3 was visible starting from the concentration of 1 μM, compound **4** induced a massive increase in acetylated tubulin already at the concentration of 0.1 μM (Figure 4a). As expected, tideglusib did not induce any effect on tubulin acetylation (Figure SI8).

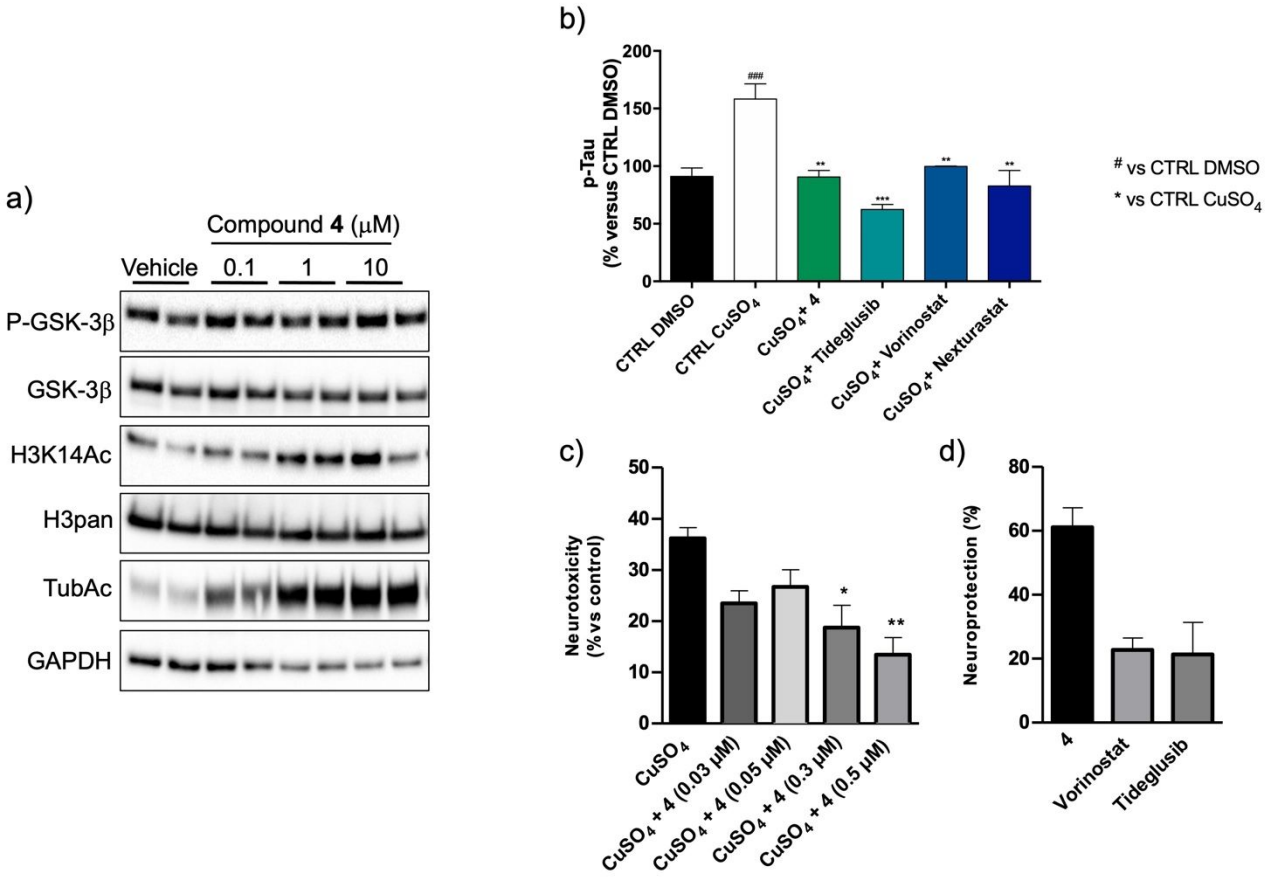

Figure 4. (a) Effect of treatment with compound **4** on GSK-3β phosphorylation, and histone H3 and alpha tubulin acetylation in SH-SY5Y cells. A Western blot analysis of phospho-GSK-3β (Ser9; P-GSK-3β), acetyl histone 3 (H3K14ac), and acetylated α-tubulin (TubAc) levels in protein extracts from SH-SY5Y cells treated with vehicle (0.1% DMSO) or different concentrations (0.1 μM, 1 μM, and 10 μM) of compound **4** for 24 h. Immunoblots are examples from two biological replicates of each experimental condition; (b) effects of the compounds on tau phosphorylation. The differentiated SH-SY5Y cells were pretreated with compounds (10 μM) for 1 h and then with $CuSO_4$ (400 μM) for 16 h. The extent of tau phosphorylation was determined through immunoenzymatic assay. Absorbance was measured at 450 nm. Values represent the means ± SEM; *$p < 0.05$, ***$p < 0.001$ vs control (CTRL); #$p < 0.05$, ##$p < 0.01$, ###$p < 0.001$ vs cells treated with $CuSO_4$; (c) effect of

compound **4** on the neurotoxicity induced by $CuSO_4$ in SH-SY5Y cells. Cells were incubated for 24 h with compound **4** (0.03, 0.05, 0.3, 0.5 μM) in the presence of $CuSO_4$ (600 μM); (d) effect of compound **4** compared to tideglusib and vorinostat; cells were incubated for 24 h with compound **4**, vorinostat or tideglusib (0.5 μM) in the presence of $CuSO_4$ (600 μM). Cell viability was measured using MTT assay as described in the experimental section. Data are expressed in terms of neurotoxicity and neuroprotection (% inhibition of neurotoxicity induced by $CuSO_4$). Data are reported as mean ± SEM of three independent experiments; *$p < 0.05$ and **$p < 0.01$ vs. cells treated with $CuSO_4$ at one-way ANOVA with Dunnett post hoc test.

Tau phosphorylation and neuroprotection. Several studies have reported that GSK-3β is involved in tau protein phosphorylation and neuronal death in AD.[30] In this regard, *in vitro* and *in vivo* studies have demonstrated the role of $CuSO_4$ to exacerbate tau hyperphosphorylation, ultimately contributing to both synaptic failure and neuronal death.[31] In this context, we evaluated the effect of compound **4** on $CuSO_4$-induced tau hyperphosphorylation and cell death. $CuSO_4$ induced a time-dependent tau phosphorylation in differentiated SH-SY5Y cells, with a peak after 16 h of incubation.[4] Based on this evidence, a 16 h treatment with $CuSO_4$ (400 μM) was used to identify the ability of the compound **4** to counteract $CuSO_4$-induced tau phosphorylation. As reported in Figure 4b, compound **4** at 10 μM concentration completely counteracted $CuSO_4$ mediated tau phosphorylation. It is interesting to note that while vorinostat is less active than compound **4**, nexturastat A shows comparable activity to compound **4**. This could be ascribed to the modest inhibitory activity showed by nexturastat A against GSK-3β, probably due to structural similarity to the GSK-3β inhibitor AR-A014418.[32] Furthermore, it is reported that selective HDAC6 inhibitors can affect tau phosphorylation by acting on several mechanisms, such as increasing GSK-3β phosphorylation on serine 9.[29, 33.34]

Then, to assess the neuroprotective effect of compound **4** on neurotoxicity induced by $CuSO_4$, SH-SY5Y cells were incubated for 24 h with compound **4** (0.03, 0.05, 0.3, 0.5 μM), vorinostat (0.5 μM), and tideglusib (0.5 μM), in the presence of $CuSO_4$ (600 μM), and cell viability was determined

through MTT assay.[24] As reported in Figure 4c, compound **4** significantly reduced the neurotoxicity evoked by $CuSO_4$ at 0.3 and 0.5 μM. It is interesting to note that the neuroprotective effects of compound **4** were dose-related (Figure 4c) and three-fold higher than the reference compounds vorinostat and tideglusib (Figure 4d).

Immunomodulatory effects. Evidence suggests that neuroinflammation and microglia-related mechanisms in Aβ clearance and production play a crucial role in the pathogenesis and progression of AD.[35] Furthermore, it has been demonstrated that HDAC isoforms and GSK-3β stimulate microglia activation.[36] Microglia may acquire two different phenotypes, pro-inflammatory M1, characterized by Nitric Oxide Synthase 2 (NOS2) upregulation and production of proinflammatory cytokines, and the neuroprotective M2 phenotype, characterized by the expression of Triggering receptor expressed on myeloid cells 2 (TREM2) and that of growth factors, such as Transforming growth factor-beta 2 (TGFβ2). M1-like microglia promote the release of various proinflammatory cytokines, thus inducing bystander tissue injury. By contrast, M2-like macrophages may actively promote tissue remodeling and repair. The immunomodulatory effect of compound **4**, in comparison with reference compounds, was determined by treating N9 microglial cells with an increasing concentration of compounds (0.1, 1, 10 μM) in the presence or absence of lipopolysaccharide (LPS, 100 ng/mL), which is an M1 state inducer. As reported in Figure 5, compound **4** leads to a significant and dose-dependent decrease in iNOS and nitric oxide expression in the medium, suggesting an immunomodulatory effect, as it significantly reduces LPS-mediated pro-inflammatory activation of microglia compared with the LPS-treated control. A similar effect was observed when cells were treated with tideglusib, while HDACIs induced a significant increase in iNOS and nitrite production at all tested concentrations, indicating increased microglia activation in the presence of the molecules compared to controls (Figure SI9). On the other hand, regarding the M2 microglia markers TREM and TGFB2, no significant differences were observed between controls and cells treated with molecules at different concentrations, ruling out the possibility of a phenotypic transition from pro-inflammatory M1 to protective M2 microglia (Figures 5 and SI9).

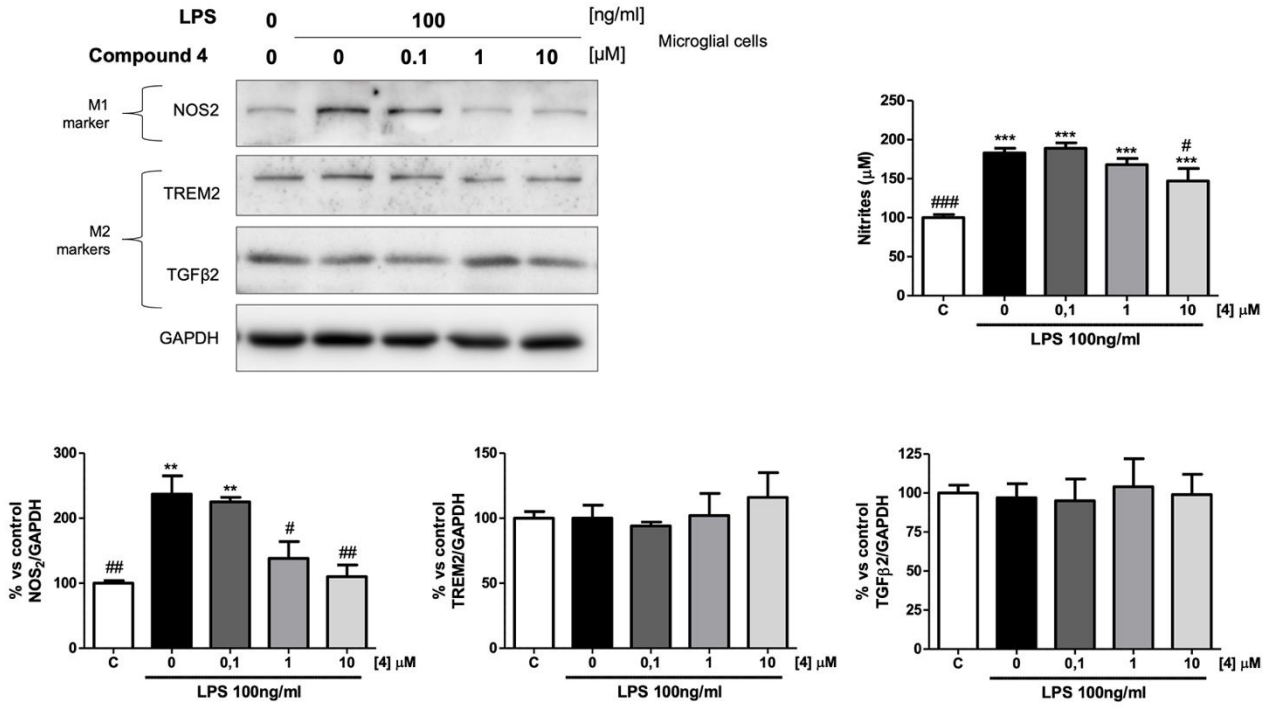

Figure 5. Effect of compound **4** on murine N9 microglial cells following induction in M1 activation state by LPS (100 ng/mL) treatment. iNOS, TREM2 and TGFβ2 expression were analyzed using Western blot after a 24 h treatment with LPS and increasing concentrations of compound **4** (0.1, 1, and 10 μM). For the indirect determination of Nitric Oxide (NO) release, nitrites derived from N9-cultured media were quantified through the Griess reaction. Values are reported as means ± SEM from three independent experiments; ** p <0.01, *** p <0.001 vs control ©; # p <0.05, ## p <0.01, ### p <0.001 vs LPS-activated microglia (0); One way ANOVA with Dunnett' post-hoc comparison test.

BBB permeability studies and in silico pharmacokinetic parameters. The ability of compound **4** to cross the Blood-Brain Barrier (BBB) was explored by performing the Parallel Artificial Membrane Permeability Assay (PAMPA). Indeed, the capacity to reach the therapeutic targets in the CNS is a critical step in the development of drugs for AD. The *in vitro* permeability (*Pe*) of compound **4** through the porcine lipid membrane was assessed in comparison to some commercial drugs used in the experiment validation (see SI). The reported Pe values for standard compounds were related to

those reported in the literature,[37, 38] after which the ability of compound **4** to permeate the BBB was predicted. Based on the *in vitro* results obtained, compound **4** was demonstrated to be potentially centrally active with a permeability (*Pe*) value of 12±1.

Furthermore, the pharmacokinetic properties and drug-likeness of compound **4** were calculated by online SwissADME.[39] Table SI2 shows that there was no Lipinski violation nor PAINS alert for compound **4**, which is not a p-GP substrate, and also possesses high gastrointestinal tract (GI) absorption. Furthermore, it shows high Ligand Efficacy against all the three target enzymes (0.49 vs GSK-3β, 0.53 vs HDAC2 and HDAC6).[40] All these results demonstrate that compound **4** have favorable drug-likeness and pharmacokinetic properties in silico.

Conclusions

In conclusion, by exploiting a classical design strategy our study has uncovered potent dual inhibitors of GSK-3β and HDAC2/6 that are able to exert anti-AD properties. The designed compounds showed high potency in *in vitro* assay and compound **4** exhibited cellular effects that are consistent with targets inhibition. Due to its activity profile, and thanks to its penetration of the BBB and favorable in silico ADMET profile, compound **4** might be considered a promising hit compound to develop, and an innovative disease-modifying agent. Hit-to-lead optimization studies, together with development of PK−PD relationships, are currently ongoing and will be reported in due course.

METHODS

Chemistry

General Experimental Procedures. All the commercially available reagents and solvents were purchased from Sigma-Aldrich, Alpha Aesar, and VWR, and used without further purification. Reactions were followed by analytical thin layer chromatography (TLC), on precoated TLC plates (layer 0.20 mm silica gel 60 with a fluorescent indicator UV254, from SigmaAldrich). Developed plates were air-dried and analyzed under a UV lamp (UV 254/365 nm). Nuclear magnetic resonance

(NMR) experiments were run on a Varian VXR deuterated dimethyl sulfoxide (DMSO-d6), and chloroform ($CDCl_3$). Chemical shifts (δ) are reported in parts per million (ppm) relative to tetramethylsilane (TMS) as the internal reference, and coupling constants (J) are reported in hertz (Hz). The spin multiplicities are reported as s (singlet), brs (broad singlet), d (doublet), t (triplet), q (quartet), and m (multiplet). Low-resolution and high-resolution mass spectra were recorded on a VG707EH-F or a Xevo G2-XS QTof apparatus, and electrospray ionization (ESI), both in positive and negative modes, was applied. All the final compounds showed ≥ 95% purity in analytical HPLC. Compounds were named following IUPAC rules as applied by ChemBioDraw Ultra (version 21.0.0).

General procedure for the synthesis of compounds 1-8. Trifluoroacetic acid was added dropwise to a solution of the appropriate THP-protected hydroxamic acid **26-33** in dichloromethane, and the resulting mixture was stirred at room temperature until disappearance of the starting material, as observed by TLC. The solvent was removed, and the resulting residue was purified via flash chromatography using a mixture of dichloromethane/methanol (from 10:0 to 9:1) as a mobile phase to provide the resulting final compounds **1-8**.

4-((3,5-dioxo-2-phenyl-1,2,4-thiadiazolidin-4-yl)methyl)-*N*-hydroxybenzamide (1). Synthesized from **26** (0.100 g, 0.23 mmol), obtained 0.031 g (39 % yield). ^{1}H-NMR (400 MHz, DMSO-d_6) δ 4.32 (s, 2H), 7.18-7.21 (m, 2H), 7.32-7.38 (m, 5H), 7.70 (d, 2H, J = 8.0 Hz), 9.06 (brs, 1H), 11.19 (brs, 1H); ^{13}C-NMR (150 MHz, DMSO-d_6) δ 42.89, 118.15, 121.56, 127.33, 127.37, 129.08, 131.66, 140.88, 144.23, 155. 72, 163.82, 165.83; HRMS (ESI): $C_{16}H_{14}N_3O_4S$ $[M + H]^+$: calcd 344.0705, found 344.0924.

4-((2-benzyl-3,5-dioxo-1,2,4-thiadiazolidin-4-yl)methyl)-N-hydroxybenzamide (2). Synthesized from **27** (0.300 g, 0.68 mmol), obtained 0.113 g (46 % yield). ^{1}H-NMR (400 MHz, DMSO-d_6) δ 4.82 (s, 4H), 7.32-7.42 (m, 7H), 7.74 (d, 2H, J = 8.4 Hz), 9.05 (brs, 1H), 11.21 (brs, 1H); ^{13}C-NMR (150 MHz,DMSO-d_6)

δ 44.92, 47.66, 127.29, 127.50, 128.15, 128.31, 128.84, 132.36, 135.47, 138.73, 152.72, 163.82, 16 5.83; HRMS (ESI): $C_{17}H_{16}N_3O_4S$ $[M + H]^+$: calcd 358.0862, found 358.0422.

4-((3,5-dioxo-2-phenethyl-1,2,4-thiadiazolidin-4-yl)methyl)-N-hydroxybenzamide (3). Synthesized from **28** (0.100 g, 0.22 mmol), obtained 0.030 g (37 % yield). ^{1}H-NMR (400 MHz, DMSO-d_6) δ 2.90 (t, 2H, J = 8.0 Hz), 3.89 (t, 2H, J = 8.0 Hz), 4.73 (s, 2H), 7.22-7.29 (m, 7H), 7.72 (d, 2H, J = 8.4 Hz), 9.04 (brs, 1H), 11.22 (brs, 1H); ^{13}C-NMR (150 MHz, DMSO-d_6) δ 33.86, 44.64, 45.35, 126.62, 127.18, 127.26, 128.44, 128.84, 132.23, 137.52, 138.66, 152.33, 163.83, 165.83; HRMS (ESI): $C_{18}H_{18}N_3O_4S$ $[M + H]^+$: calcd 372.1018, found 372.1375.

N-hydroxy-4-((2-(naphthalen-1-yl)-3,5-dioxo-1,2,4-thiadiazolidin-4-yl)methyl)benzamide (4). Synthesized from **29** (0.160 g, 0.34 mmol), obtained 0.100 g (74 % yield). ^{1}H-NMR (400 MHz, DMSO-d_6) δ 4.94 (s, 2H), 7.47-7.49 (m, 2H), 7.61-7.68 (m, 3H), 7.77-7.82 (m, 3H), 7.91-7.95 (m, 1H), 8.07-8.11 (m, 2H), 9.05 (brs, 1H), 11.23 (brs, 1H); ^{13}C-NMR (150 MHz, DMSO-d_6) δ 45.34, 122.43, 125.81, 127.00, 127.31, 127.57, 127.64, 127.94, 128.60, 129.00, 130.14, 131.05, 132.35, 133.99, 138.71, 151.95, 163.91, 166.10; HRMS (ESI): $C_{20}H_{16}N_3O_4S$ $[M + H]^+$: calcd 394.0862, found 394.1134.

N-hydroxy-4-((2-(4-methoxyphenyl)-3,5-dioxo-1,2,4-thiadiazolidin-4-yl)methyl)benzamide (5). Synthesized from **30** (0.110 g, 0.24 mmol), obtained 0.045 g (41 % yield). ^{1}H-NMR (400 MHz, DMSO-d_6) δ 3.78 (s, 3H), 4.86 (s, 2H), 7.02 (d, 2H, J = 8.4 Hz), 7.42-7.73 (m, 4H), 7.74 (d, 2H, J = 8.4 Hz)), 9.04 (brs, 1H), 11.21 (brs, 1H); ^{13}C-NMR (150 MHz, DMSO-d_6) δ 45.08, 55.47, 114.66, 126.74, 127.24, 127.58, 128.07, 132.33, 138.61, 151.07, 158.41, 163.87, 165.30; HRMS (ESI): $C_{17}H_{16}N_3O_5S$ $[M + H]^+$: calcd 374.0811, found 374.1003.

4-((3,5-dioxo-2-(p-tolyl)-1,2,4-thiadiazolidin-4-yl)methyl)-N-hydroxybenzamide (6). Synthesized from **31** (0.098 g, 0.22 mmol), obtained 0.027 g (34 % yield). ^{1}H-NMR (400 MHz, DMSO-d_6) δ 2.32 (s, 3H), 4.87 (s, 2H), 7.28 (d, 2H, J = 8.8 Hz), 7.42-7.45 (m, 4H), 7.74 (d, 2H, J = 8.4 Hz), 9.04 (brs, 1H), 11.21 (brs, 1H); ^{13}C-NMR (150 MHz, DMSO-d_6) δ 20.51, 45.07, 123.92, 123.96, 127.25, 127.59, 129.92, 133.22, 136.72, 138.57, 150.74, 163.87, 165.09; HRMS (ESI): $C_{17}H_{16}N_3O_4S$ $[M + H]^+$: calcd 358.0862, found 358.0744.

4-((3,5-dioxo-2-(4-(trifluoromethyl)phenyl)-1,2,4-thiadiazolidin-4-yl)methyl)-N-hydroxybenzamide (7). Synthesized from **32** (0.115 g, 0.23 mmol), obtained 0.040 g (42 % yield). ^{1}H-NMR (400 MHz, DMSO-d_6) δ 4.89 (s, 2H), 7.45 (d, 2H, J = 8.4 Hz), 7.74 (d, 2H, J = 8.2 Hz), 7.81-7.87 (m, 4H), 9.03 (brs, 1H), 11.22 (brs, 1H); HRMS (ESI): $C_{17}H_{13}F_3N_3O_4S$ $[M + H]^+$: calcd 412.0579, found 412.0867.

4-((2-(4-chlorophenyl)-3,5-dioxo-1,2,4-thiadiazolidin-4-yl)methyl)-N-hydroxybenzamide (8). Synthesized from **33** (0.087 g, 0.18 mmol), obtained 0.050 g (74 % yield). ^{1}H-NMR (400 MHz, DMSO-d_6) δ 4.48 (s, 2H), 7.31 (d, 2H, J = 8.4 Hz), 7.45-7.55 (m, 4H), 7.89 (d, 2H, J = 8.2 Hz), 9.06 (brs, 1H), 11.17 (brs, 1H); ^{13}C-NMR (150 MHz, DMSO-d_6) δ 46.11, 123.86, 123.91, 127.11, 127.44, 130.01, 133.07, 136.44, 138.30, 150.43, 164.04, 165.33; HRMS (ESI): $C_{16}H_{13}ClN_3O_4S$ $[M + H]^+$: calcd 378.0315, found 378.0527.

General procedure for the synthesis of compounds 10-17. A stirred solution of isothiocyanate **9** and the corresponding commercially available isocyanate in THF (5 mL) was cooled to 0 °C and sulfuryl chloride (1 M solution in DCM) was added slowly. The mixture was allowed to warm to room temperature and stirred for 12 h. After this time, the reaction was then opened to the air and stirred for 30 minutes before the solvent was removed, and the resulting residue was purified via flash chromatography using a mixture of petroleum ether/ethyl acetate (from 10:0 to 9:1) as a mobile phase to provide the resulting compounds **10-17**.

Tert-butyl 4-((3,5-dioxo-2-phenyl-1,2,4-thiadiazolidin-4-yl)methyl)benzoate (10). Synthesized from **9** (0.300 g, 1.20 mmol), phenylisocyanate (0.143 g, 1.20 mmol) and sulfuryl dichloride (1.2 ml); obtained 0.165 g (36 % yield). ^{1}H-NMR (400 MHz, DMSO-d_6) δ 1.58 (s, 9H), 4.90 (s, 2H), 6.75-6.90 (m, 2H), 7.16-7.35 (m, 5H), 7.72 (d, 2H, J = 8.0 Hz).

Tert-butyl 4-((2-benzyl-3,5-dioxo-1,2,4-thiadiazolidin-4-yl)methyl)benzoate (11). Synthesized from **9** (0.450 g, 1.81 mmol), benzylisocyanate (0.240 g, 1.81 mmol) and sulfuryl dichloride (3.60 ml); obtained 0.300 g (42 % yield). ^{1}H-NMR (400 MHz, DMSO-d_6) δ 1.54 (s, 9H), 4.77 (s, 2H), 4.89 (s, 2H), 7.00 (d, 2H, J = 8.8 Hz), 7.41-7.45 (m, 5H), 7.75 (d, 2H, J = 8.4 Hz).

Tert-butyl 4-((3,5-dioxo-2-phenethyl-1,2,4-thiadiazolidin-4-yl)methyl)benzoate (12). Synthesized from **9** (0.764 g, 3.1 mmol), phenethylisocyanate (0.456 g, 3.1 mmol) and sulfuryl dichloride (3 ml); obtained 0.610 g (43 % yield). ^{1}H-NMR (400 MHz, DMSO-d_6) δ 1.64 (s, 9H), 2.90 (t, 2H, J = 7.2 Hz), 3.91 (t, 2H, J = 7.2 Hz), 4.95 (s, 2H), 7.17-7.33 (m, 7H), 7.70 (d, 2H, J = 8.4 Hz).

Tert-butyl 4-((2-(naphthalen-1-yl)-3,5-dioxo-1,2,4-thiadiazolidin-4-yl)methyl)benzoate (13). Synthesized from **9** (0.500 g, 0.20 mmol), 1-naphthylisocyanate (0.372 g, 0.20 mmol) and sulfuryl dichloride (3 ml); obtained 0.510 g (51 % yield). ^{1}H-NMR (400 MHz, DMSO-d_6) δ 1.53 (s, 9H), 4.94 (s, 2H), 7.51 (d, 2H, J = 8.4 Hz), 7.59-7.65 (m, 3H), 7.77-7.79 (m, 2H), 7.92 (d, 2H, J = 8.4 Hz), 8.05-8.10 (m, 1H).

tert-butyl 4-((2-(4-methoxyphenyl)-3,5-dioxo-1,2,4-thiadiazolidin-4-yl)methyl)benzoate (14). Synthesized from **9** (0.860 g, 0.34 mmol), methoxyphenylisocyanate (0.510 g, 0.34 mmol) and sulfuryl dichloride (3.45 ml); obtained 0.610 g (43 % yield). ^{1}H-NMR (400 MHz, DMSO-d_6) δ 1.60 (s, 9H), 3.76 (s, 3H), 4.93 (s, 2H), 6.91 (d, 2H, J = 8.8 Hz), 7.22 (d, 2H, J = 8.4 Hz), 7.37 (d, 2H, J = 9.2 Hz), 7.96 (d, 2H, J = 8.4 Hz).

Tert-butyl 4-((3,5-dioxo-2-(p-tolyl)-1,2,4-thiadiazolidin-4-yl)methyl)benzoate (15). Synthesized from **9** (0.500 g, 2 mmol) and p-tolylisocyanate (0.266 g, 2 mmol) and sulfuryl dichloride (4.0 ml); obtained 0.240 g (29 % yield). ^{1}H-NMR (400 MHz, DMSO-d_6) δ 1.53 (s, 9H), 2.32 (s, 3H), 4.87 (s, 2H), 7.29 (d, 2H, J = 8.8 Hz), 7.41-7.47 (m, 4H), 7.74 (d, 2H, J = 8.4 Hz).

Tert-butyl 4-((3,5-dioxo-2-(4-(trifluoromethyl)phenyl)-1,2,4-thiadiazolidin-4-yl)methyl)benzoate (16). Synthesized from **9** (0.430 g, 1.73 mmol) and 4-(trifluoromethyl)phenylisocyanate (0.323 g, 1.73 mmol) and sulfuryl dichloride (1.73 ml); obtained 0.600 g (77 % yield). ^{1}H-NMR (400 MHz, DMSO-d_6) δ 1.49 (s, 9H), 4.88 (s, 2H), 7.41 (d, 2H, J = 8.4 Hz), 7.79 (d, 2H, J = 8.2 Hz), 7.84-7.88 (m, 4H).

tert-butyl 4-((2-(4-chlorophenyl)-3,5-dioxo-1,2,4-thiadiazolidin-4-yl)methyl)benzoate (17). Synthesized from **9** (0.330 g, 1.32 mmol) and 4-chlorophenylisocyanate (0.203 g, 1.32 mmol) and

sulfuryl dichloride (2.65 ml); obtained 0.195 g (35 % yield). ^{1}H-NMR (400 MHz, DMSO-d_6) δ 1.51 (s, 9H), 4.46 (s, 2H), 7.27 (d, 2H, J = 8.4 Hz), 7.47-7.54 (m, 4H), 7.92 (d, 2H, J = 8.2 Hz).

General procedure for the synthesis of compounds 18-25. Trifluoracetic acid was added to a stirred solution of the protected acid **10-17** in dichloromethane, and the resulting mixture was stirred at room temperature for 12h. The organic solution was washed with water (2 times), then brine and dried to give **10-17** as solid, that were used in the following steps without further purification.

4-((3,5-dioxo-2-phenyl-1,2,4-thiadiazolidin-4-yl)methyl)benzoic acid (18). Synthesized from **10** (0.165 g, 0.43 mmol) and 1.5 ml of trifluoracetic acid; obtained 0.059 g (41 % yield). ^{1}H-NMR (400 MHz, DMSO-d_6) δ 4.91 (s, 2H), 7.46-7.50 (m, 5H), 7.58 (d, 2H, J = 8.4 Hz), 7.94 (d, 2H, J = 8.4 Hz).

4-((2-benzyl-3,5-dioxo-1,2,4-thiadiazolidin-4-yl)methyl)benzoic acid (19). Synthesized from **11** (0.200 g, 0.50 mmol) and 2.0 ml of trifluoracetic acid; obtained 0.130 g (76 % yield). ^{1}H-NMR (400 MHz, DMSO-d_6) δ 4.80 (s, 2H), 4.94 (s, 2H), 7.08 (d, 2H, J = 8.2 Hz), 7.46-7.50 (m, 5H), 7.99 (d, 2H, J = 8.4 Hz).

4-((3,5-dioxo-2-phenethyl-1,2,4-thiadiazolidin-4-yl)methyl)benzoic acid (20). Synthesized from **12** (0.300 g, 0.7 mmol) and 5.0 ml of trifluoracetic acid; obtained 0.197 g (79 % yield). ^{1}H-NMR (400 MHz, DMSO-d_6) δ 2.92 (t, 2H, J = 7.0 Hz), 3.97 (t, 2H, J = 7.0 Hz), 4.99 (s, 2H), 7.11-7.25 (m, 7H), 7.74 (d, 2H, J = 8.4 Hz).

4-((2-(naphthalen-1-yl)-3,5-dioxo-1,2,4-thiadiazolidin-4-yl)methyl)benzoic acid (21). Synthesized from **13** (0.500 g, 1.1 mmol) and 5.0 ml of trifluoracetic acid; obtained 0.213 g (51 % yield). ^{1}H-NMR (400 MHz, DMSO-d_6) δ 4.92 (s, 2H), 7.44 (d, 2H, J = 8.4 Hz), 7.51-7.56 (m, 3H), 7.78-7.80 (m, 1H), 7.90-7.92 (m, 1H), 7.95 (d, 2H, J = 8.4 Hz), 8.07-8.10 (m, 2H).

4-((2-(4-methoxyphenyl)-3,5-dioxo-1,2,4-thiadiazolidin-4-yl)methyl)benzoic acid (22). Synthesized from **14** (0.630 g, 1.5 mmol) and 5.3 ml of trifluoracetic acid; obtained 0.315 g (58 % yield). ^{1}H-NMR (400 MHz, DMSO-d_6) δ 3.73 (s, 3H), 4.90 (s, 2H), 6.98 (d, 2H, J = 8.4 Hz), 7.33 (d, 2H, J = 8.4 Hz), 7.39 (d, 2H, J = 8.8 Hz), 7.91 (d, 2H, J = 8.4 Hz).

4-((3,5-dioxo-2-(p-tolyl)-1,2,4-thiadiazolidin-4-yl)methyl)benzoic acid (23). Synthesized from **15** (0.240 g, 0.60 mmol) and 3.0 ml of trifluoracetic acid; obtained 0.150 g (73 % yield). ^{1}H-NMR (400 MHz, DMSO-d_6) δ 2.37 (s, 3H), 4.96 (s, 2H), 7.27 (d, 2H, J = 8.8 Hz), 7.39-7.48 (m, 4H), 7.76 (d, 2H, J = 8.4 Hz).

4-((3,5-dioxo-2-(4-(trifluoromethyl)phenyl)-1,2,4-thiadiazolidin-4-yl)methyl)benzoic acid (24). Synthesized from **16** (0.500 g, 1.11 mmol) and 4.0 ml of trifluoracetic acid; obtained 0.370 g (84 % yield). ^{1}H-NMR (400 MHz, DMSO-d_6) δ 4.90 (s, 2H), 7.39 (d, 2H, J = 8.4 Hz), 7.83 (d, 2H, J = 8.2 Hz), 7.81-7.87 (m, 4H).

4-((2-(4-chlorophenyl)-3,5-dioxo-1,2,4-thiadiazolidin-4-yl)methyl)benzoic acid (25). Synthesized from **17** (0.140 g, 0.33 mmol) and 2.0 ml of trifluoracetic acid; obtained 0.105 g (86 % yield). ^{1}H-NMR (400 MHz, DMSO-d_6) δ 4.83 (s, 2H), 7.40 (d, 2H, J = 8.4 Hz), 7.44-7.54 (m, 4H), 7.77 (d, 2H, J = 8.0 Hz).

General procedure for the synthesis of compounds 26-33. EDCI and HOBT were added to a stirred solution of the corresponding acid **18-25** in anhydrous dimethylformamide at 0 °C and under a stream of nitrogen, and the resulting mixture was stirred for 30 minutes. After this, o-(Tetrahydro-2H-pyran-2-yl)hydroxylamine was added and the resulting mixture was stirred at rt for 12h. Water was added and the mixture was extracted with dichloromethane (3 times). The organic layers were collected, washed with brine and dried over sodium sulphate to give a residue that was purified via flash chromatography using a mixture of petroleum ether/ethyl acetate (from 10:0 to 9:1) as a mobile phase to provide the resulting compounds **26-33**.

4-((3,5-dioxo-2-phenyl-1,2,4-thiadiazolidin-4-yl)methyl)-N-((tetrahydro-2H-pyran-2-yl)oxy)benzamide (26). Synthesized from **18** (0.200 g, 0.60 mmol) and o-(Tetrahydro-2H-pyran-2-yl)hydroxylamine (0.071 g, 0.60 mmol); obtained 0.120 g (47 % yield). ^{1}H-NMR (400 MHz, DMSO-d_6) δ 1.48-1.53 (m, 3H), 1.61-1.66 (m, 3H), 3.52-3.56 (m, 1H), 3.96-4.00 (m, 1H), 4.93 (s, 2H), 4.97-5.01 (m, 1H), 7.39-7.45 (m, 5H), 7.61 (d, 2H, J = 8.4 Hz), 7.89 (d, 2H, J = 8.4 Hz).

4-((2-benzyl-3,5-dioxo-1,2,4-thiadiazolidin-4-yl)methyl)-N-((tetrahydro-2H-pyran-2-yl)oxy)benzamide (27). Synthesized from **19** (0.250 g, 0.70 mmol) and o-(Tetrahydro-2H-pyran-2-yl)hydroxylamine (0.085 g, 0.70 mmol); obtained 0.135 g (44 % yield). ^{1}H-NMR (400 MHz, DMSO-d_6) δ 1.46-1.51 (m, 3H), 1.62-1.68 (m, 3H), 3.50-3.54 (m, 1H), 3.99-4.04 (m, 1H), 4.29 (s, 2H), 4.76 (s, 2H), 4.98-5.02 (m, 1H), 7.21-7.24 (m, 2H), 7.29-7.35 (m, 5H), 7.75 (d, 2H, J = 8.0 Hz).

4-((3,5-dioxo-2-phenethyl-1,2,4-thiadiazolidin-4-yl)methyl)-N-((tetrahydro-2H-pyran-2-yl)oxy)benzamide (28). Synthesized from **20** (0.167 g, 0.47 mmol) and o-(Tetrahydro-2H-pyran-2-yl)hydroxylamine (0.055 g, 0.47 mmol); obtained 0.110 g (51 % yield). ^{1}H-NMR (400 MHz, DMSO-d_6) δ 1.51-1.56 (m, 3H), 1.68-1.74 (m, 3H), 2.88 (t, 2H, J = 6.8 Hz), 3.49-3.52 (m, 1H), 3.83 (t, 2H, J = 7.2 Hz), 4.00-4.06 (m, 1H), 4.72 (s, 2H), 4.95-4.99 (m, 1H), 7.21-7.27 (m, 7H), 7.70 (d, 2H, J = 8.4 Hz).

4-((2-(naphthalen-1-yl)-3,5-dioxo-1,2,4-thiadiazolidin-4-yl)methyl)-N-((tetrahydro-2H-pyran-2-yl)oxy)benzamide (29). Synthesized from **21** (0.213 g, 0.56 mmol), EDCI (0.214 g, 1.11 mmol), HOBT (0.076 g, 0.56 mmol) and o-(Tetrahydro-2H-pyran-2-yl)hydroxylamine (0.065 g, 0.56 mmol); obtained 0.160 g (60 % yield). ^{1}H-NMR (400 MHz, DMSO-d_6) δ 1.49-1.54 (m, 3H), 1.71-1.77 (m, 3H), 3.46-3.51 (m, 1H), 4.03-4.07 (m, 1H), 4.79 (s, 2H), 4.92-4.96 (m, 1H), 7.47 (d, 2H, J = 8.4 Hz), 7.55-7.62 (m, 3H), 7.77-7.83 (m, 1H), 7.92-7.95 (m, 1H), 7.98 (d, 2H, J = 8.4 Hz), 8.06-8.09 (m, 2H).

4-((2-(4-methoxyphenyl)-3,5-dioxo-1,2,4-thiadiazolidin-4-yl)methyl)-N-((tetrahydro-2H-pyran-2-yl)oxy)benzamide (30). Synthesized from **22** (0.148 g, 0.41 mmol) and o-(Tetrahydro-2H-pyran-2-yl)hydroxylamine (0.048 g, 0.41 mmol); obtained 0.160 g (85 % yield). ^{1}H-NMR (400 MHz, DMSO-d_6) δ 1.51-1.55 (m, 3H), 1.65-1.69 (m, 3H), 3.66-3.75 (m, 1H), 3.81 (s, 3H), 3.99-4.03 (m, 1H), 4.85 (s, 2H), 4.93-4.99 (m, 1H), 7.00 (d, 2H, J = 9.2 Hz), 7.41-7.47 (m, 4H), 7.73 (d, 2H, J = 8.4 Hz).

4-((3,5-dioxo-2-(p-tolyl)-1,2,4-thiadiazolidin-4-yl)methyl)-N-((tetrahydro-2H-pyran-2-yl)oxy)benzamide (31). Synthesized from **23** (0.125 g, 0.36 mmol) and o-(Tetrahydro-2H-pyran-2-yl)hydroxylamine (0.043 g, 0.36 mmol); obtained 0.098 g (62 % yield). ^{1}H-NMR (400 MHz, DMSO-

d$_6$) δ 1.46-1.51 (m, 3H), 1.59-1.63 (m, 3H), 2.44 (s, 3H), 3.59-3.65 (m, 1H), 3.87-3.94 (m, 1H), 4.77 (s, 2H), 4.82-4.86 (m, 1H), 7.19 (d, 2H, J = 8.8 Hz), 7.34-7.45 (m, 4H), 7.82 (d, 2H, J = 8.4 Hz).

4-((3,5-dioxo-2-(4-(trifluoromethyl)phenyl)-1,2,4-thiadiazolidin-4-yl)methyl)-N-((tetrahydro-2H-pyran-2-yl)oxy)benzamide (32). Synthesized from **24** (0.570 g, 1.44 mmol) and o-(Tetrahydro-2H-pyran-2-yl)hydroxylamine (0.168 g, 1.44 mmol); obtained 0.374 g (52 % yield). ^{1}H-NMR (400 MHz, DMSO-*d*$_6$) δ 1.43-1.48 (m, 3H), 1.58-1.64 (m, 3H), 3.63-3.67 (m, 1H), 3.89-3.94 (m, 1H), 4.93 (s, 2H), 4.99-5.03 (m, 1H), 7.42 (d, 2H, J = 8.4 Hz), 7.78 (d, 2H, J = 8.2 Hz), 7.83-7.88 (m, 4H).

4-((2-(4-chlorophenyl)-3,5-dioxo-1,2,4-thiadiazolidin-4-yl)methyl)-N-((tetrahydro-2H-pyran-2-yl)oxy)benzamide (33). Synthesized from **25** (0.105 g, 0.29 mmol) and o-(Tetrahydro-2H-pyran-2-yl)hydroxylamine (0.034 g, 0.29 mmol); obtained 0.087 g (65 % yield). ^{1}H-NMR (400 MHz, DMSO-*d*$_6$) δ 1.51-1.54 (m, 3H), 1.67-1.73 (m, 3H), 3.48-3.52 (m, 1H), 3.99-4.04 (m, 1H), 4.86 (s, 2H), 4.91-4.97 (m, 1H), 7.43 (d, 2H, J = 8.4 Hz), 7.52-7.61 (m, 4H), 7.73 (d, 2H, J = 8.0 Hz).

GSK-3β inhibition in vitro assay. Human recombinant GSK-3β, prephosphorylated polypeptide substrate and white 96-well plates were purchased from Millipore (Millipore Iberica S.A.U.). Kinase-Glo Luminescent Kinase Assay was obtained from Promega (Promega Biotech Iberica, SL). Adenosinetriphosphate (ATP) and all other reagents were from Sigma-Aldrich (Sigma-Aldrich St Louis, MO, USA). Assay buffer contained 50 mM 4-(2-hydroxyethyl)-1- piperazineethanesulfonic acid (HEPES) (pH 7.5), 1 mM ethylenediaminetetraacetic acid (EDTA), 1 mM ethylene glycol tetraacetic acid (EGTA), and 15 mM magnesium acetate. The in solution experiments for the GSK-3β inhibition analysis were performed following the method developed by Baki et al.[41] In a typical assay, 10 μL of test compound (dissolved in DMSO at 1 mM concentration and diluted in advance in assay buffer to the desired concentration) and 10 μL (20 ng) of enzyme were added to each well in presence of 20 μL of assay buffer containing GSM substrate and ATP in order to reach a 25 μM and 1 μM final concentration, respectively. The final DMSO percentage in the reaction mixture did not exceed 1%. After a 30 min incubation time at 37 °C, the enzymatic reaction was stopped by adding 40 μL of Kinase-Glo reagent. Glow-type luminescence was recorded after 10 min using a Victorx3

(PerkinElmer Waltham, MA, USA) plate reader. The activity was found proportional to the difference of the total and consumed ATP. The inhibitory activities were calculated based on maximal kinase (average positive) and luciferase activities (average negative) measured in the absence of inhibitor and in the presence of reference compound inhibitor (SB-415286 Merck Millipore, IC_{50} = 55 nM) at the total inhibition concentration (5 μM), respectively. The linear regression parameters were determined and the IC_{50} was extrapolated using GraphPad software (version 9.0; GraphPad Software, La Jolla, CA, USA).

Kinetic Studies on GSK-3β. To investigate the inhibitory mechanism of compound **4**, Lineweaver−Burk double-reciprocal plots of enzyme kinetics were obtained. The kinetic experiments varying both GSM (from 6.25 to 50 μM) and **4** (from 25 to 100 nM) concentrations were carried out. Kinetic experiments were also conducted varying both ATP (from 1 to 50 μM) and **4** (from 50 to 125 nM) concentrations. All the experiments were performed using the ATP-Glo Kinase Assay.

HDAC inhibition in vitro assay. HDAC2 and HDAC6 isoforms were purchased from VinciBiochem (VinciBiochem, FI, Italy). White 96-well plates were purchased from Millipore (Millipore Iberica S.A.U.). HDAC-Glo (TM) I/II Assay kit, was obtained from Promega (Promega Biotech Iberica, SL). A bioluminogenic assay was used to monitor the activity of HDAC2 and HDAC6 enzymes. A proluminogenic substrate containing an acetylated lysine peptide sequence derived from histone 4 conjugated to aminoluciferin was applied. HDAC enzyme–mediated deacetylation of the lysine residue facilitates luminogenic substrate susceptibility to specific proteolytic cleavage by the enzyme contained in the developer reagent.[42] The aminoluciferin product obtained from the cleavage is a substrate for luciferase, and the amount of light produced in this reaction is proportional to enzyme activities. The HDAC-Glo I/II assay reagent was prepared by i) rehydration of lyophilized HDAC-Glo I/II substrate (with an acetylated peptide concentration of 100 μM) in 10 mL HDAC-Glo I/II assay buffer and ii) addition of 10 μL of developer reagent (containing trypsin). The % of inhibition as well as the IC_{50} values for both standard inhibitors and **1-8** compounds towards each enzyme were determined by diluting HDAC enzymes as appropriate, using the HDAC-

Glo I/II assay buffer. 25 μL of solution containing enzyme was dispensed into microtiter plates. Then the same volume of HDAC-Glo I/II assay buffer in the absence of tested compounds (activity) and in the presence of inhibitors at desired concentrations was added. After a 30 min incubation time at 37 °C, the enzymatic reaction was stopped by adding 50 μL of developer reagent prepared as reported previously. The microtiter plate was mixed briefly through orbital shaking (500–700 rpm), and luminescence was measured after 15 min using a Victorx3 (PerkinElmer Waltham, MA, USA) plate reader. For inhibitor concentration-response experiments, the IC_{50} values were calculated by fitting the duplicate data in GraphPad Prism (version 9.0; GraphPad Software, La Jolla, CA, USA).

HDAC K_i determination. Assays were performed as previously described and were performed in 96-well plates (Fischer Scientific, cat. #: 3686) in HEPES buffer (50 mM HEPES, 100 mM KCl, 0.001% Tween-20 (v/v), 0.2 mM TCEP, pH 7.4 at 25 °C; 25 μL/well final volume) added bovine serum albumin (BSA; Sigma-Aldrich #A3059; 0.5 mg/mL for HDAC1, HDAC2, HDAC3, HDAC4, HDAC5, HDAC6, HDAC7, HDAC8, HDAC9 and 0.05 mg/mL for HDAC11). Inhibitors (4-fold dilution series starting from concentrations at either 50 or 10 μM) were incubated with enzyme (HDAC1 [5 nM], HDAC2 [2 nM], HDAC3 [1 nM], HDAC4 [0.05 nM], HDAC5 [0.10 nM], HDAC6 [1 nM], HDAC7 [0.05 nM], HDAC8 [0.5 nM], HDAC9 [0.10 nM], HDAC11 [0.5 nM]) and substrates (HDAC1, 2, 3 and 6: Ac-Leu-Gly-Lys(Ac)-AMC (20 μM), HDAC4, 5, 7, 8 and 9: Ac-Leu-Glu-Lys(TFA)-AMC (20 μM for HDAC4, 120 μM for HDAC5, 40 μM for HDAC7, 100 μM for HDAC8 and 80 μM for HDAC9), HDAC11: Ac-Glu-Thr-Asp-Lys(Myr)-AMC (50 μM) were incubated for 30 min at 37 °C (AMC = 7-amino-4-methylcoumarin) before a solution of trypsin (Sigma-Aldrich #T8003; 25 μL, 0.4 mg/mL; final concentration 0.2 mg/mL) was subsequently added, and the assay was allowed to develop for 15 min at room temperature. Then fluorescence was recorded on a plate reader (FLUOstar Omega) with excitation at 360 nm and detecting emission at 460 nm. Data was analysed to afford residual enzymatic activity relative to control wells and, assuming fast-on/fast-off mechanism, IC_{50} values were obtained by fitting the results to the dose-

response equation with a variable Hill-slope. Inhibition K_i values were calculated from the Cheng-Prusoff equation and reported substrate K_M-values (HDAC1: K_M = 5.4 μM[43], HDAC2: K_M = 6.1 μM[43], HDAC3: K_M = 5.4 μM[43], HDAC4: K_M = 10.3 μM[44], HDAC5: K_M = 59 μM[44], HDAC6 K_M = 16 μM[44], HDAC7: K_M = 19.8 μM[44], HDAC8 K_M = 190 μM[44], HDAC9: K_M = 37 μM[44], HDAC11 K_M = 62 μM[45]). Assays were performed at least twice with in plate duplicates, and data was analysed using GraphPad Prism. Enzyme source: HDAC1: BPS Bioscience #50051 (Full length with C-terminal His6 and FLAG tag); HDAC2: BPS Bioscience #50052 (Full length with C-terminal FLAG-tag); HDAC3: BPS Bioscience #50003 (Full length with C-terminal HIS-tag in complex with human NCOR2 395-489 with C-terminal GST-tag); HDAC4: BPS Bioscience #50004 (Catalytic domain (627-1084) with N-terminal GST-tag and C-terminal His-tag); HDAC5: BPS Bioscience #50005 (Catalytic domain (656-1122) with C-terminal His-tag); HDAC6: BPS Bioscience #50056 (Full length with C-terminal FLAG-tag); HDAC7: BPS Bioscience #50007 (Catalytic domain (518-end) with N-terminal GST-tag); HDAC8: BPS Bioscience #50008 (Full length with C-terminal His-tag); HDAC9: BPS Bioscience #50009 (Catalytic domain (604-1066) with C-terminal His-tag); HDAC11: BPS Bioscience #50021 (Full length untagged).

$$v_i = v_{bottom} + \frac{v_{top} - v_{bottom}}{1 + 10^{(\log IC_{50} - \log[I])h}}$$

$$K_i = \frac{IC_{50}}{1 + \frac{[S]}{K_M}}$$

PAMPA BBB permeation studies. Atenolol, caffeine, imipramine, testosterone, estradiol, and progesterone were purchased from Sigma Aldrich (Sigma-Aldrich St Louis, MO, USA) and used as reference compounds for PAMPA development and validation. Phosphate buffer saline solution at pH 7.4 (PBS), ethanol, and dodecane were purchased from Sigma Aldrich. The porcine polar brain lipid, used for the preparation of the lipid membrane, was from Avanti Polar Lipids (Alabaster, AL, USA). The donor plate was a 96-well filter plate (Multiscreen® IP Sterile Plate PDVF membrane, pore size 0.45 μM, catalog no. MAIPS4510) and the acceptor plate was an indented 96-well plate

(Multiscreen®, catalog no. MAMCS9610) both from Millipore (Millipore Iberica S.A.U.). Prediction of brain penetration was evaluated using the PAMPA assay.[37] Test compounds (1-2 mg of atenolol, caffeine, imipramine, testosterone, estradiol, progesterone, and compound **4**) were dissolved in EtOH to obtain 10 mM solutions and then diluted to reach the concentration of 500 μM in a final volume of 2.5 mL containing 70% PBS pH=7.4 and 30% of ethanol. The acceptor 96-well microplate was filled with 200 μL of PBS/EtOH (70:30). The donor 96-well plate was coated with 4 μL of porcine brain lipid in dodecane (20 mg mL^{-1}) and, after 10 min, 200 μL of each compound solution was added. Then, the donor plate was carefully put onto the acceptor plate to form a "sandwich", which was left undisturbed for 2 h 45 min at 37 °C under constant slight shaking (50 rpm). During this time the compounds diffused from the donor plate through the lipid membrane into the acceptor plate. After incubation, the donor plate was removed. The solution in the acceptor plate corresponding with each compound was collected and the UV absorbance was determined through spectrophotometer. Results are given as the standard error of the mean (SEM) and the average of two experiments. 6 quality control compounds (previously mentioned) of known intestinal permeability were included in each experiment to validate the analysis set.

The permeability coefficient (*Pe*) of each drug, in centimeters per second, was calculated by applying the following formula

$$Pe = \frac{Vd \cdot Vr}{(Vd + Vr) \cdot S \cdot t} ln \frac{100 \cdot Vd}{100 \cdot Vd - \%T(Vd + Vr)}$$

$$\%T = \frac{\mathrm{Vr} \cdot \mathrm{Ar}}{Ad_0 \cdot \mathrm{Vd}} 100$$

in which Vd and Vr are the volumes of the donor and the receptor solutions (0.20 cm^3), S is the membrane area (0.266 cm^2), t is the incubation time (12600sg), Ar is the absorbance of the receptor plate solutions after the experiment, and Ad_0 is the initial absorbance in the donor compartment.

Computational analysis.

To perform the docking study, we looked for HDAC-2 and HDAC-6 X-ray structures available in PDB, with similar co-crystalized hydroxamate compounds like those presented here. For HDAC2, the best resolution human complex with vorinostat (PDB ID: 4LXZ)[46] was chosen, whereas for human HDAC6 only one structure co-crystallized with trichostatin A (TSA) (PDB ID: 5EDU)[47] was available in the PDB. Given the difficulties in reproducing the crystallographic poses of vorinostat in HDAC2 and trichostatin A in HDAC6, we performed docking simulation by constraining the position of the hydroxamate group. Both cognate ligands (vorinostat and trichostatin A) present a hydroxamate group moiety that coordinates the zinc ion in a bidentate manner, and that we retained in all simulations.

The binding site residue tautomeric states and the ligand protonation were set according to the enzyme mechanism of action and to the information available in literature. Thus, all compounds were docked as deprotonated hydroxamates. The catalytic histidines were modelled as protonated, in the case of His145 (HDAC2) and His610 (HDAC6), and neutral as HYD tautomer for His146 (HDAC2) and His611 (HDAC6).

The docking simulations were performed through Maestro induced-fit docking XP procedure, generating 10 different poses for each derivative, and selecting the docking pose with the highest Glide Emodel score as the most representative.

Biology

MTT Assay. Human neuroblastoma SH-SY5Y cells, deriving from The European Collection of Authenticated Cell Cultures (Sigma-Aldrich, St. Louis, MO, USA) were maintained in Dulbecco modified Eagle medium (DMEM, Thermo Fisher Scientific, Waltham, MA, USA) supplemented with 10% heat-inactivated FBS, 2 mM of glutamine, and antibiotics (penicillin, 100 U/mL; streptomycin, 100 μg/mL, Thermo Fisher Scientific, Waltham, MA, USA), in a humidified atmosphere of 5% of CO_2 at 37 °C. Cell medium was replaced every 3 days and the cells were sub-cultured once they reached 90% confluence. Cell viability was detected using MTT assay (Sigma-Aldrich, USA). SH-SY5Y cells were cultured in a 96-well plate at a density of 5×10^4 cells per well in culture medium

supplemented with 10% FBS. The following day, cells were treated with compound **4**, nexurastat A, vorinostat, tideglusib, or vehicle (0.1% DMSO) with different concentrations at 0.1 μM, 1 μM, 10 μM, 25 μM, 50 μM, and 100 μM for 24 h. A total of 10 μL MTT solution (5 mg/mL in phosphate-buffered solution) was added to each well and the plate was incubated for 4 h at 37 °C in a CO_2 incubator. The MTT solution was removed from the wells by aspiration and the formazan crystals were dissolved in DMSO. Finally, the intensity of the dissolved formazan crystals (purple color) was quantified using the microplate reader at 540 nm. All experiments were performed in triplicate.

Western Blotting. SH-SY5Y cells were treated with compound **4**, nexurastat A, vorinostat, tideglusib, or vehicle (0.1% DMSO) at 0.1 μM, 1 μM, and 10 μM, for 24h. For the preparation of total cell extracts, cells were lysed in ice-cold RIPA buffer (50 mM Tris–HCl, pH 7.4, 150 mM NaCl, 1% Triton-X100, 0.5% sodium deoxycholate, 0.1% SDS) supplemented with 1mM PMSF, and with 1% protease and phosphatase inhibitor cocktail (Sigma-Aldrich, St. Louis, MO, USA). Protein concentration was determined using the Bradford method. Equivalent amounts of protein (50 μg) were subjected to electrophoresis on a Bolt™ 4 to 12%, Bis-Tris gel (Invitrogen™) and transferred to a Hybond-ECL nitrocellulose membrane (Amersham-GE Healthcare Life Sciences, Chicago, IL, USA). For acetylated tubulin detection, 10 μg of proteins were loaded onto the gel. The primary and secondary antibodies used are listed in Supplementary Table 2. To quantify post-translational modifications, such as phosphorylation and acetylation, the nitrocellulose membranes were stripped in Restore Western Blot Stripping Buffer (Thermo Fisher Scientific, Waltham, MA, USA) for 20 min and reprobed with the corresponding total protein antibody. The densitometric analysis of digitized Western blot images was performed using Chemidoc XRS Imaging Systems and the Image LabTM Software (Bio-Rad); this software automatically highlights any saturated pixels of the Western blot images in red. Images acquired with exposition times that generated protein signals out of a linear range were not considered for the quantification.

Determination of neuroprotection. SH-SY5Y cells were seeded in a 96-well plate at 2×10^4 cells/well, incubated for 24 h and then treated with compound **4** (0.03-0.5 μM), vorinostat (0.03-0.5

μM), and tideglusib (0.5-10 μM) for 24 h in the presence of $CuSO_4$ (600 μM). At the end of the treatment, cell viability was evaluated by the reduction of MTT to its insoluble formazan. Briefly, the treatment was replaced with MTT in HBSS (0.5 mg/mL) for 2 h at 37 °C in 5% CO_2. After washing with HBSS, formazan crystals were dissolved in isopropanol. The amount of formazan was measured (570 nm, reference filter 690 nm) using a multilabel plate reader (VICTOR™ X3). Neurotoxicity is expressed as a percentage of control cells and calculated using the formula: 100 – ((absorbance of treated neurons/absorbance of untreated neurons) × 100)). Neuroprotection is expressed as a percentage of inhibition of neurotoxicity induced by $CuSO_4$ and calculated using the formula: 100 – ((% neurotoxicity with compound and $CuSO_4$/% neurotoxicity with $CuSO_4$) × 100)). Data are shown as means ± standard error (SEM) of at least three independent experiments. Statistical analysis was performed using one-way ANOVA with the Dunnett post hoc test. Differences were considered significant at $p < 0.05$. Analyses were performed using GraphPad PRISM software (version 5.0; GraphPad Software, La Jolla, CA, USA) on a Windows platform.

Intracellular p-tau content in neuronal cells. A neuroblastoma cell line, SH-SY5Y, was cultured in DMEM-F12 medium supplemented with 15% fetal bovine serum (FBS), 1% non-essential amino acids (NEAA), 2 mM L-glutamine (L-glu), and penicillin/streptomycin (Pen/Strep) and maintained at 37°C in a humidified atmosphere (5% CO_2). SH-SY5Y cells were differentiated by supplementing the DMEM-F12 medium with 1% FBS, 2 mL L-glu, and 5 μM retinoic acid (RA) for seven days.[4] On the sixth day, the differentiated cells were pre-treated with 1% DMSO (as a control) or 10 μM compounds (i.e., 10 μM compound **4**, 10 μM Tideglusib, 10 μM Vorinostat, or 10 μM Nexturastat) for 1 hour. Subsequently, 400 μM of copper (II) sulfate solution ($CuSO_4$ in water) was incubated for 16 hours, since it has been proposed to be a great inductor of tau phosphorylation.[20] At the end of the differentiation and treatment period, the cells were detached from the culture plate and lysed by adding 200 μL of lysis buffer with protease inhibitors. The total protein concentration was assessed using Bradford assay. Next, the concentration of p-tau was assessed using a home-made immunoenzymatic assay, as similarly described.[4] Briefly, wells were pre-coated with a full-length

antibody to tau (sc-32274, Santa Cruz Biotechnology, diluted 1:100) and incubated overnight at room temperature. Then, the non-specific sites were blocked by using bovine serum albumin (BSA) for 90 minutes at 37 °C. The lysed cells (30 μg of total proteins/100 μL) were added to wells for 90 minutes at 25 °C. After extensive washes with phosphate buffered saline containing 0.01% Tween 20 (PBS-T), a rabbit polyclonal antibody directed against p-tau (Proteintech, #28866-1-AP, diluted 1:500) was incubated for 90 minutes at 37°C. Afterwards, an anti-rabbit-HRP secondary antibody was employed. Finally, the wells were washed three times before adding the enzyme substrate 3,3′,5,5′-tetramethylbenzidine (TMB, Thermo Scientific), thus allowing the colorful reaction to develop. An H_2SO_4 solution was added to stop the reaction and the absorbance was read at 450 nm.

Immunomodulation. Mouse N9 microglial cells were cultured in Dulbecco Modified Eagle Medium (DMEM) supplemented with 10% heat-inactivated Fetal Bovine Serum (FBS), 1% Penicillin/Streptomycin and 2mM Glutamine (all from Aurogene, Rome, Italy). Once confluent, cells were washed with PBS (0.9% NaCl in 50mM phosphate buffer pH 7.4) and incubated with Trypsin – EDTA solution (Sigma-Aldrich, St Louis, MO, USA) 4 min at 37°C. An equal volume of complete DMEM medium was then added to inhibit the trypsin reaction, and cells were collected and centrifugated at 300g for 5min. For experiments, microglial cells were counted by using the BLAUBRAND® Neubauer chamber and 2.5 x 105 cells/ 35mm ø Petri dish were plated in complete DMEM medium w/o FBS and exposed to 100ng/mL lipopolysaccharide (LPS), which induces M1 activation, and an increasing concentration of compounds (0.1, 1, 10μM). After 24 h of treatment, conditioned media were collected, and nitrites formed by spontaneous oxidation of Nitric Oxide (NO) were spectrophotometrically detected based on the Griess assay. In parallel, microglial cells were collected in lysis buffer (1% SDS, 50mM Tris-HCL pH 7.4, 1mM EDTA, 10μl/mL protease and phosphatase inhibitors) and the expression of the inducible Nitric Oxide Synthase (iNOS; M1 pro-inflammatory microglia marker), TREM2 and TGFβ2 (markers of myeloid-phagocytic, and therefore anti-inflammatory, M2 microglia) was analysed using Western Blot. GAPDH was used for endogenous normalization.

ASSOCIATED CONTENT

Supporting Information

The Supporting Information is available free of charge at. This includes: characterization of compounds and supplementary figures (PDF).

AUTHOR INFORMATION

Corresponding author

Angela De Simone - Department of Drug Science and Technology, University of Turin, Via Pietro Giuria 9, 10125 Torino, Italy; Email: angela.desimone@unito.it

Andrea Milelli - Department for Life Quality Studies, Alma Mater Studiorum-University of Bologna, Corso d'Augusto 237, 47921 Rimini, Italy. orcid.org/0000-0003-2285-7403; Email: andrea.milelli3@unibo.it

Author Contributions

A.S, R.S, V.T and A.M. performed chemical synthesis and compounds characterization; E.T, V.A, D.D., C.A.O. and A.D.S. performed enzymatic in vitro assay; M.L., E.C., S.T., E.P., R.P., S.D., C.M., B.P. and A.T. performed cell-based assay; M.B. and F.S. performed computational studies; A.M. conceived the idea, supervised the work, and wrote the manuscript with contributions by all co-authors. All authors have given approval to the final version of the manuscript.

Notes

The authors declare no competing financial interest.

ACKNOWLEDGMENTS

This research was supported by the University of Bologna (Grant RFO and ALMA IDEA 2022 - NextGenerationEU), PRA_2022_60 Ateneo Project of University of Pisa, Next Generation EU – National Recovery and Resilience Plan (Piano Nazionale di Ripresa e Resilienza, NRRP) – Mission 4 Component 2 Investment 1.4 – Ministry of University and Research (MUR) Call N. 3277 Project Code ECS_00000017 MUR Directoral Decree n.1055 , 23 June 2022, CUP B83C22003930001,

project title “Tuscany Health Ecosystem – THE”, Spoke 8, University of Turin (SPY_RILO_21_01, SPY_RILO_22_01) and Independent Research Fund Denmark–Technical and Production Sciences (0136-00412B, C.A.O.)

ABBREVIATIONS

Aβ, amyloid β; AD, Alzheimer’s Disease; BBB, Blood Brain Barrier; CDKL5, Cyclin-Dependent Kinase-like 5; GSK-3β, Glycogen Synthase Kinase 3β; HDAC, Histone Deacetylase; MTDs, Multitarget Drugs; NOS2, Nitric Oxide Synthase 2; TGFβ2, Transforming Growth Factor- β 2; TREM2, Triggering receptor.

Bibliography

(1) Cummings, J.; Lee, G.; Nahed, P.; Kambar, M. E. Z. N.; Zhong, K.; Fonseca, J.; Taghva, K. Alzheimer's disease drug development pipeline: 2022. *Alzheimers Dement (N Y)* **2022**, *8* (1), e12295. DOI: 10.1002/trc2.12295.
(2) Oset-Gasque, M. J.; Marco-Contelles, J. Alzheimer's Disease, the "One-Molecule, One-Target" Paradigm, and the Multitarget Directed Ligand Approach. *ACS Chem Neurosci* **2018**. DOI: 10.1021/acschemneuro.8b00069.
(3) Bolognesi, M. L. Harnessing Polypharmacology with Medicinal Chemistry. *ACS Med Chem Lett* **2019**, *10* (3), 273-275. DOI: 10.1021/acsmedchemlett.9b00039.
(4) De Simone, A.; La Pietra, V.; Betari, N.; Petragnani, N.; Conte, M.; Daniele, S.; Pietrobono, D.; Martini, C.; Petralla, S.; Casadei, R.; et al. Discovery of the First-in-Class GSK-3β/HDAC Dual Inhibitor as Disease-Modifying Agent To Combat Alzheimer's Disease. *ACS Med Chem Lett* **2019**, *10* (4), 469-474. DOI: 10.1021/acsmedchemlett.8b00507.
(5) De Simone, A.; Milelli, A. Histone Deacetylase Inhibitors as Multitarget Ligands: New Players in Alzheimer's Disease Drug Discovery? *ChemMedChem* **2019**, *14* (11), 1067-1073. DOI: 10.1002/cmdc.201900174.
(6) Llorens-Martín, M.; Jurado, J.; Hernández, F.; Avila, J. GSK-3β, a pivotal kinase in Alzheimer disease. *Front Mol Neurosci* **2014**, *7*, 46. DOI: 10.3389/fnmol.2014.00046.
(7) De Simone, A.; Tumiatti, V.; Andrisano, V.; Milelli, A. Glycogen Synthase Kinase 3β: A New Gold Rush in Anti-Alzheimer's Disease Multitarget Drug Discovery? *J Med Chem* **2021**, *64* (1), 26-41. DOI: 10.1021/acs.jmedchem.0c00931.
(8) Kremer, A.; Louis, J. V.; Jaworski, T.; Van Leuven, F. GSK3 and Alzheimer's Disease: Facts and Fiction…. *Front Mol Neurosci* **2011**, *4*, 17. DOI: 10.3389/fnmol.2011.00017.
(9) Giese, K. P. GSK-3: a key player in neurodegeneration and memory. *IUBMB Life* **2009**, *61* (5), 516-521. DOI: 10.1002/iub.187.
(10) Penney, J.; Tsai, L. H. Histone deacetylases in memory and cognition. *Sci Signal* **2014**, *7* (355), re12. DOI: 10.1126/scisignal.aaa0069.
(11) Li, Y.; Lin, S.; Gu, Z.; Chen, L.; He, B. Zinc-dependent deacetylases (HDACs) as potential targets for treating Alzheimer's disease. *Bioorg Med Chem Lett* **2022**, *76*, 129015. DOI: 10.1016/j.bmcl.2022.129015.

(12) Avila, J.; León-Espinosa, G.; García, E.; García-Escudero, V.; Hernández, F.; Defelipe, J. Tau Phosphorylation by GSK3 in Different Conditions. *Int J Alzheimers Dis* **2012**, *2012*, 578373. DOI: 10.1155/2012/578373.
(13) Green, H. F.; Nolan, Y. M. GSK-3 mediates the release of IL-1β, TNF-α and IL-10 from cortical glia. *Neurochem Int* **2012**, *61* (5), 666-671. DOI: 10.1016/j.neuint.2012.07.003.
(14) Guan, J. S.; Haggarty, S. J.; Giacometti, E.; Dannenberg, J. H.; Joseph, N.; Gao, J.; Nieland, T. J.; Zhou, Y.; Wang, X.; Mazitschek, R.; et al. HDAC2 negatively regulates memory formation and synaptic plasticity. *Nature* **2009**, *459* (7243), 55-60. DOI: 10.1038/nature07925.
(15) Canter, R. G.; Penney, J.; Tsai, L. H. The road to restoring neural circuits for the treatment of Alzheimer's disease. *Nature* **2016**, *539* (7628), 187-196. DOI: 10.1038/nature20412. Zhang, L.; Liu, C.; Wu, J.; Tao, J. J.; Sui, X. L.; Yao, Z. G.; Xu, Y. F.; Huang, L.; Zhu, H.; Sheng, S. L.; et al. Tubastatin A/ACY-1215 improves cognition in Alzheimer's disease transgenic mice. *J Alzheimers Dis* **2014**, *41* (4), 1193-1205. DOI: 10.3233/JAD-140066.
(16) Fischer, A.; Sananbenesi, F.; Mungenast, A.; Tsai, L. H. Targeting the correct HDAC(s) to treat cognitive disorders. *Trends Pharmacol Sci* **2010**, *31* (12), 605-617. DOI: 10.1016/j.tips.2010.09.003. Sharma, S.; Sarathlal, K. C.; Taliyan, R. Epigenetics in Neurodegenerative Diseases: The Role of Histone Deacetylases. *CNS Neurol Disord Drug Targets* **2019**, *18* (1), 11-18. DOI: 10.2174/1871527317666181004155136.
(17) Pao, P. C.; Patnaik, D.; Watson, L. A.; Gao, F.; Pan, L.; Wang, J.; Adaikkan, C.; Penney, J.; Cam, H. P.; Huang, W. C.; et al. HDAC1 modulates OGG1-initiated oxidative DNA damage repair in the aging brain and Alzheimer's disease. *Nat Commun* **2020**, *11* (1), 2484. DOI: 10.1038/s41467-020-16361-y.
(18) Bardai, F. H.; Price, V.; Zaayman, M.; Wang, L.; D'Mello, S. R. Histone deacetylase-1 (HDAC1) is a molecular switch between neuronal survival and death. *J Biol Chem* **2012**, *287* (42), 35444-35453. DOI: 10.1074/jbc.M112.394544.
(19) Chen, S.; Owens, G. C.; Makarenkova, H.; Edelman, D. B. HDAC6 regulates mitochondrial transport in hippocampal neurons. *PLoS One* **2010**, *5* (5), e10848. DOI: 10.1371/journal.pone.0010848.
(20) Cook, C.; Stankowski, J. N.; Carlomagno, Y.; Stetler, C.; Petrucelli, L. Acetylation: a new key to unlock tau's role in neurodegeneration. *Alzheimers Res Ther* **2014**, *6* (3), 29. DOI: 10.1186/alzrt259.
(21) Loi, M.; Gennaccaro, L.; Fuchs, C.; Trazzi, S.; Medici, G.; Galvani, G.; Mottolese, N.; Tassinari, M.; Giorgini, R. R.; Milelli, A.; et al. Treatment with a GSK-3β/HDAC Dual Inhibitor Restores Neuronal Survival and Maturation in an In Vitro and In Vivo Model of. *Int J Mol Sci* **2021**, *22* (11). DOI: 10.3390/ijms22115950.
(22) Martinez, A.; Alonso, M.; Castro, A.; Pérez, C.; Moreno, F. J. First non-ATP competitive glycogen synthase kinase 3 beta (GSK-3beta) inhibitors: thiadiazolidinones (TDZD) as potential drugs for the treatment of Alzheimer's disease. *J Med Chem* **2002**, *45* (6), 1292-1299.
(23) del Ser, T.; Steinwachs, K. C.; Gertz, H. J.; Andrés, M. V.; Gómez-Carrillo, B.; Medina, M.; Vericat, J. A.; Redondo, P.; Fleet, D.; León, T. Treatment of Alzheimer's disease with the GSK-3 inhibitor tideglusib: a pilot study. *J Alzheimers Dis* **2013**, *33* (1), 205-215. DOI: 10.3233/JAD-2012-120805.
(24) Guardigni, M.; Pruccoli, L.; Santini, A.; Simone, A.; Bersani, M.; Spyrakis, F.; Frabetti, F.; Uliassi, E.; Andrisano, V.; Pagliarani, B.; et al. PROTAC-Induced Glycogen Synthase Kinase 3β Degradation as a Potential Therapeutic Strategy for Alzheimer's Disease. *ACS Chem Neurosci* **2023**, *14* (11), 1963-1970. DOI: 10.1021/acschemneuro.3c00096.
(25) Bergman, J. A.; Woan, K.; Perez-Villarroel, P.; Villagra, A.; Sotomayor, E. M.; Kozikowski, A. P. Selective histone deacetylase 6 inhibitors bearing substituted urea linkers inhibit melanoma cell growth. *J Med Chem* **2012**, *55* (22), 9891-9899. DOI: 10.1021/jm301098e.
(26) Martinez, A.; Alonso, M.; Castro, A.; Dorronsoro, I.; Gelpí, J. L.; Luque, F. J.; Pérez, C.; Moreno, F. J. SAR and 3D-QSAR studies on thiadiazolidinone derivatives: exploration of structural

requirements for glycogen synthase kinase 3 inhibitors. *J Med Chem* **2005**, *48* (23), 7103-7112. DOI: 10.1021/jm040895g.
(27) https://www.rcsb.org. *access date: 01/03/2023*.
(28) Bahmad, H. F.; Chalhoub, R. M.; Harati, H.; Bou-Gharios, J.; Assi, S.; Ballout, F.; Monzer, A.; Msheik, H.; Araji, T.; Elajami, M. K.; et al. Tideglusib attenuates growth of neuroblastoma cancer stem/progenitor cells in vitro and in vivo by specifically targeting GSK-3β. *Pharmacol Rep* **2021**, *73* (1), 211-226. DOI: 10.1007/s43440-020-00162-7.
(29) Fan, S. J.; Huang, F. I.; Liou, J. P.; Yang, C. R. The novel histone de acetylase 6 inhibitor, MPT0G211, ameliorates tau phosphorylation and cognitive deficits in an Alzheimer's disease model. *Cell Death Dis* **2018**, *9* (6), 655. DOI: 10.1038/s41419-018-0688-5.
(30) Lauretti, E.; Dincer, O.; Praticò, D. Glycogen synthase kinase-3 signaling in Alzheimer's disease. *Biochim Biophys Acta Mol Cell Res* **2020**, *1867* (5), 118664. DOI: 10.1016/j.bbamcr.2020.118664.
(31) Zubčić, K.; Hof, P. R.; Šimić, G.; Jazvinšćak Jembrek, M. The Role of Copper in Tau-Related Pathology in Alzheimer's Disease. *Front Mol Neurosci* **2020**, *13*, 572308. DOI: 10.3389/fnmol.2020.572308.
(32) Bhat, R.; Xue, Y.; Berg, S.; Hellberg, S.; Ormö, M.; Nilsson, Y.; Radesäter, A. C.; Jerning, E.; Markgren, P. O.; Borgegård, T.; et al. Structural insights and biological effects of glycogen synthase kinase 3-specific inhibitor AR-A014418. *J Biol Chem* **2003**, *278* (46), 45937-45945. DOI: 10.1074/jbc.M306268200.
(33) Trzeciakiewicz, H.; Ajit, D.; Tseng, J. H.; Chen, Y.; Ajit, A.; Tabassum, Z.; Lobrovich, R.; Peterson, C.; Riddick, N. V.; Itano, M. S.; et al. An HDAC6-dependent surveillance mechanism suppresses tau-mediated neurodegeneration and cognitive decline. *Nat Commun* **2020**, *11* (1), 5522. DOI: 10.1038/s41467-020-19317-4.
(34) Noack, M.; Leyk, J.; Richter-Landsberg, C. HDAC6 inhibition results in tau acetylation and modulates tau phosphorylation and degradation in oligodendrocytes. *Glia* **2014**, *62* (4), 535-547. DOI: 10.1002/glia.22624.
(35) Leng, F.; Edison, P. Neuroinflammation and microglial activation in Alzheimer disease: where do we go from here? *Nat Rev Neurol* **2021**, *17* (3), 157-172. DOI: 10.1038/s41582-020-00435-y.
(36) Durham, B. S.; Grigg, R.; Wood, I. C. Inhibition of histone deacetylase 1 or 2 reduces induced cytokine expression in microglia through a protein synthesis independent mechanism. *J Neurochem* **2017**, *143* (2), 214-224. DOI: 10.1111/jnc.14144.
(37) Di, L.; Kerns, E. H.; Fan, K.; McConnell, O. J.; Carter, G. T. High throughput artificial membrane permeability assay for blood-brain barrier. *Eur J Med Chem* **2003**, *38* (3), 223-232.
(38) Yuskaitis, C. J.; Jope, R. S. Glycogen synthase kinase-3 regulates microglial migration, inflammation, and inflammation-induced neurotoxicity. *Cell Signal* **2009**, *21* (2), 264-273. DOI: 10.1016/j.cellsig.2008.10.014.
(39) Daina, A.; Michielin, O.; Zoete, V. SwissADME: a free web tool to evaluate pharmacokinetics, drug-likeness and medicinal chemistry friendliness of small molecules. *Sci Rep* **2017**, *7*, 42717. DOI: 10.1038/srep42717.
(40) Hopkins, A. L.; Groom, C. R.; Alex, A. Ligand efficiency: a useful metric for lead selection. *Drug Discov Today* **2004**, *9* (10), 430-431. DOI: 10.1016/S1359-6446(04)03069-7.
(41) Baki, A.; Bielik, A.; Molnár, L.; Szendrei, G.; Keserü, G. M. A high throughput luminescent assay for glycogen synthase kinase-3beta inhibitors. *Assay Drug Dev Technol* **2007**, *5* (1), 75-83. DOI: 10.1089/adt.2006.029.
(42) Halley, F.; Reinshagen, J.; Ellinger, B.; Wolf, M.; Niles, A. L.; Evans, N. J.; Kirkland, T. A.; Wagner, J. M.; Jung, M.; Gribbon, P.; et al. A bioluminogenic HDAC activity assay: validation and screening. *J Biomol Screen* **2011**, *16* (10), 1227-1235. DOI: 10.1177/1087057111416004.

(43) Moreno-Yruela, C.; Olsen, C. A. Determination of Slow-Binding HDAC Inhibitor Potency and Subclass Selectivity. *ACS Med Chem Lett* **2022**, *13* (5), 779-785. DOI: 10.1021/acsmedchemlett.1c00702.
(44) Bradner, J. E.; West, N.; Grachan, M. L.; Greenberg, E. F.; Haggarty, S. J.; Warnow, T.; Mazitschek, R. Chemical phylogenetics of histone deacetylases. *Nat Chem Biol* **2010**, *6* (3), 238-243. DOI: 10.1038/nchembio.313.
(45) Moreno-Yruela, C.; Galleano, I.; Madsen, A. S.; Olsen, C. A. Histone Deacetylase 11 Is an ε-N-Myristoyllysine Hydrolase. *Cell Chem Biol* **2018**, *25* (7), 849-856.e848. DOI: 10.1016/j.chembiol.2018.04.007.
(46) Lauffer, B. E.; Mintzer, R.; Fong, R.; Mukund, S.; Tam, C.; Zilberleyb, I.; Flicke, B.; Ritscher, A.; Fedorowicz, G.; Vallero, R.; et al. Histone deacetylase (HDAC) inhibitor kinetic rate constants correlate with cellular histone acetylation but not transcription and cell viability. *J Biol Chem* **2013**, *288* (37), 26926-26943. DOI: 10.1074/jbc.M113.490706.
(47) Hai, Y.; Christianson, D. W. Histone deacetylase 6 structure and molecular basis of catalysis and inhibition. *Nat Chem Biol* **2016**, *12* (9), 741-747. DOI: 10.1038/nchembio.2134.

Graphical Abstract

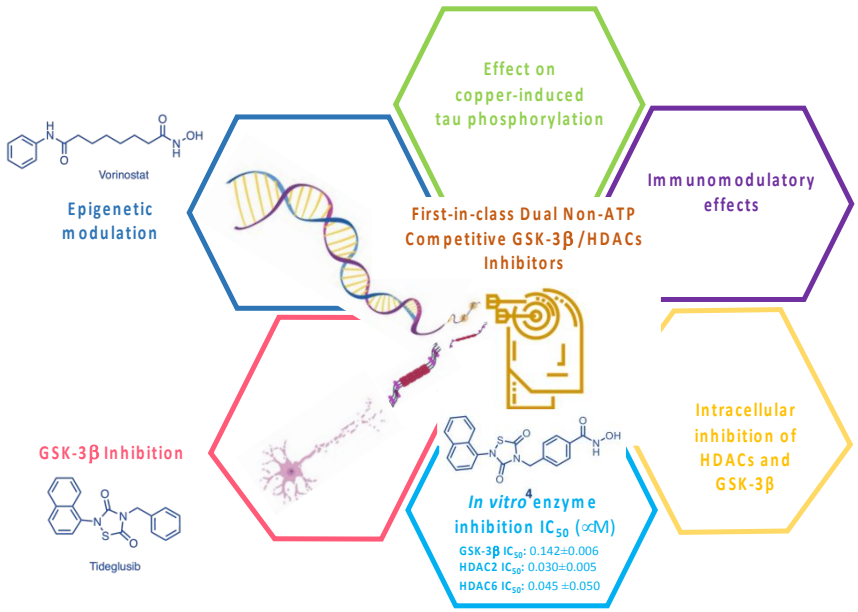
Effect on copper-induced tau phosphorylation
Immunomodulatory effects
Intracellular inhibition of HDACs and GSK-3β
In vitro[4] enzyme inhibition IC50 (∝M)
GSK-3β IC50: 0.142±0.006
HDAC2 IC50: 0.030±0.005
HDAC6 IC50: 0.045 ±0.050
GSK-3β Inhibition
Tideglusib
Epigenetic modulation
Vorinostat
First-in-class Dual Non-ATP Competitive GSK-3β /HDACs Inhibitors